Functional studies of CpSRP54 in diatoms show that the mechanism of thylakoid protein insertion differs from plants and green algae

Marianne Nymark, Marthe Caroline Grønbech Hafskjold, Charlotte Volpe, Davi de Miranda Fonseca, Animesh Sharma, Eirini Tsirvouli, Manuel Serif, Per Winge, Giovanni Finazzi, Atle Magnar Bones

Functional studies of CpSRP54 in diatoms show that the mechanism of thylakoid protein insertion differs from plants and green algae.

Marianne Nymark#[1], Marthe Caroline Grønbech Hafskjold[1,2], Charlotte Volpe[2], Davi de Miranda Fonseca[3,4], Animesh Sharma[3,4], Eirini Tsirvouli[1] Manuel Serif[1], Per Winge[1], Giovanni Finazzi[5], Atle Magnar Bones[1]

[1]Department of Biology, Norwegian University of Science and Technology, N-7491, Trondheim, Norway

[2]Department of Biotechnology and Food Science, Norwegian University of Science and Technology, N-7491, Trondheim, Norway

[3]Department of Clinical and Molecular Medicine, Norwegian University of Science and Technology, NTNU, N-7491 Trondheim, Norway

[4]Proteomics and Modomics Experimental Core Facility (PROMEC), NTNU and Central Administration, St Olavs Hospital, The University Hospital in Trondheim, Norway

[5]Universite´Grenoble Alpes (UGA), Laboratoire de Physiologie Cellulaire et Végétale, UMR 5168, Centre National de la Recherche Scientifique (CNRS), Commissariat à l'Energie Atomique et aux Energies Alternatives (CEA), Institut National de la Recherche Agronomique (INRA), Interdisciplinary Research Institute of Grenoble (IRIG), CEA-Grenoble, 38000 Grenoble, France

Running title: Effects of loss of CpSRP54 in diatoms

Summary

The chloroplast signal recognition particle 54 kDa (CpSRP54) protein is a member of the CpSRP pathway known to target proteins to thylakoid membranes in plants and green algae. Loss of CpSRP54 in the marine diatom *Phaeodactylum tricornutum* lowers the accumulation of a selection of chloroplast encoded subunits of photosynthetic complexes, indicating a role in the co-translational part of the CpSRP pathway. In contrast to plants/green algae, absence of CpSRP54 does not have a negative effect on the content of light-harvesting antenna complex proteins and pigments in *P. tricornutum*, indicating that the diatom CpSRP54 protein has not evolved to function in the post-translational part of the CpSRP pathway. *Cpsrp54* knockout mutants display altered photophysiological responses, with a stronger induction of photoprotective mechanisms and lower growth rates compared to wild type when exposed to increased light intensities. Nonetheless, their phenotype is relatively mild, thanks to activation of mechanisms alleviating the loss of CpSRP54, involving upregulation of chaperones. We conclude that plants, green algae and diatoms have evolved differences in the pathways for co-translational and post-translational insertion of proteins into the thylakoid membranes.

Introduction

Diatoms (Bacillariophyceae) are a species-rich group of unicellular, photosynthetic eukaryotes found in freshwaters and oceans worldwide, which are of enormous ecological relevance (Armbrust, 2009). This group of phytoplankton functions as a primary source of food for many aquatic organisms and is responsible for performing similar levels of photosynthetic fixation of carbon as all terrestrial rainforests combined (Nelson *et al.*, 1995, Armbrust, 2009, Gilbert *et al.*, 2009). Diatoms are also promising organisms for a multitude of potential applications within the bio-, nano- and environmental technologies (Bozarth *et al.*, 2009, Mishra *et al.*, 2017, Butler *et al.*, 2020). However, their role in primary production and potential for industrial applications is not matched by the level of basic knowledge of their photosynthetic machinery. Although the photosynthetic apparatus of Viridiplantae and Heterokonts such as diatoms share many common features, they are separated from a common ancestor by more than a billion years of evolution (Hohmann-Marriott and Blankenship, 2011). Diatoms arose by a secondary endosymbiotic event and as a result their chloroplasts are surrounded by four membranes (Gibbs, 1981, Flori *et al.*, 2016). Instead of having thylakoids organized into grana stacks interconnected by stroma-exposed lamellae typical for land plants and green algae, diatom thylakoids are organized in stacked bands of three thylakoids each, spanning along the entire

length of the plastid (Gibbs, 1970, Grouneva *et al.*, 2013). Photosystem II (PSII), cytochrome b_6f ($Cytb_6f$), photosystem I (PSI) and ATP synthase are multi-subunit protein complexes embedded in the thylakoid membranes and responsible for photosynthetic electron transport and ATP synthesis together with protein-bound and mobile electron carriers (Nelson and Ben-Shem, 2004). Light energy is collected and delivered to PSs by light harvesting complexes (LHCs) consisting of pigments and pigment-binding proteins. While the pigment-binding proteins of diatoms and plants/green algae belong to the LHC protein (LHCP) superfamily, they bind different pigments (Grossman *et al.*, 1995, Dittami *et al.*, 2010). The LHCPs of the green lineages (LHCa and LHCb) bind mainly Chl *a* and Chl *b*, whereas diatoms contain a different subfamily of LHCPs that in addition to Chl *a* also bind Chl *c* and fucoxanthin (Fx) and are therefore called Fx-Chl *a/c*-binding proteins (FCPs). The photosynthetic apparatus of eukaryotic organisms is composed of proteins encoded by both nucleus and chloroplast localized genes. In Viridiplantae, the nucleus encoded LHCPs and selected chloroplast encoded proteins are guided to thylakoid membranes by the Chloroplast Signal Recognition Particle (CpSRP) pathway (Kirst and Melis, 2014, Jeong *et al.*, 2017, Ziehe *et al.*, 2017, Ziehe *et al.*, 2018). The CpSRP54 GTPase of the CpSRP pathway has a dual function in plants and targets proteins both post-translationally (LHCPs) and co-translationally (chloroplast-encoded thylakoid membrane proteins) to thylakoids in cooperation with other members of the pathway (Pilgrim *et al.*, 1998, Amin *et al.*, 1999, Rutschow *et al.*, 2008, Hristou *et al.*, 2019). In contrast to the universally conserved SRP54 protein that plays an essential role in mediating co-translational targeting of newly synthesized proteins to cellular membranes across all kingdoms of life, the function of plant CpSRP54 is not dependent on an SRP RNA (Träger *et al.*, 2012, Ziehe *et al.*, 2017). In the post-translational pathway of plants, CpSRP54 is part of the LHCP-CpSRP43-CpSRP54-CpFTSY complex that guides LHCPs from the chloroplast membrane to the thylakoid membrane, where the ALBINO3 (ALB3) insertase mediates protein insertion (Ziehe *et al.*, 2018). In the co-translational pathway, CpSRP54 interacts with nascent polypeptides and targets translating ribosomes to thylakoid membranes (Nilsson *et al.*, 1999, Nilsson and van Wijk, 2002, Piskozub *et al.*, 2015, Hristou *et al.*, 2019). Differences in the function of CpSRP54 have been reported between plants and green algae. The *Chlamydomonas reinhardtii* CpSRP54 does not form a complex with the plastid specific chaperon CpSRP43 and is not involved in LHCP recognition, but is believed to function downstream of CpSRP43 together with its receptor CpFTSY in the posttranslational pathway (Dünschede *et al.*, 2015, Jeong *et al.*, 2017). In both plants and green algae *cpsrp54* knock out mutants, loss of CpSRP54 causes decreased levels of LHCPs and, consequently, lower pigment levels and paler green

coloration than in their wild type counterparts (Amin *et al.*, 1999, Rutschow *et al.*, 2008, Jeong *et al.*, 2017, Hristou *et al.*, 2019). *Arabidopsis thaliana* CpSRP54 co-translationally associates with a range of different subunits of the photosynthetic electron transport chain complexes, but a similar function has not been reported in *C. reinhardtii* (Nilsson *et al.*, 1999, Nilsson and van Wijk, 2002, Piskozub *et al.*, 2015, Jeong *et al.*, 2017, Hristou *et al.*, 2019). In diatoms, homologues of CpSRP54, CpFTSY and two variants of ALB3 (ALB3a and ALB3b) have been identified, whereas CpSRP43 homologues are absent (Träger *et al.*, 2012, Nymark *et al.*, 2019). In addition, the LHCP translocation defect protein (LTD), which forwards LHCPs from the chloroplast import machinery to the CpSRP complex in plants and green algae is apparently also missing in diatom genomes (Ouyang *et al.*, 2011, Jeong *et al.*, 2018). A chloroplast encoded SRP RNA is present in most, but not all diatom genomes sequenced to date (Träger *et al.*, 2012, Brembu *et al.*, 2014). Information from gene models available at NCBI and The Marine Microbial Eukaryote Meta/transcriptome Sequencing Project (MMETSP) database reveal that the CpSRP54, CpFTSY and ALB3 proteins are widespread in all algae, including red algae, haptophytes and the SAR (Stramenopila, Alveolata, and Rhizaria) clade. The LTD and CpSRP43 related proteins are probably restricted to the green lineage, even though some CpSRP43-like ankyrin-repeat proteins can be found in red algae, haptophytes, and in several species within the SAR clade. The CpSRP43-like ankyrin-repeat proteins are missing in Bolidophyceae and diatoms.

The function of ALB3b was recently investigated in the model diatom *Phaeodactylum tricornutum,* where loss of the insertase caused a striking change in cell color from brown to green (Nymark *et al.*, 2019). The change in pigmentation was caused by a ~75% decrease of the main group of FCP proteins (LHCFs) and a subsequent lowered level of antenna pigments (including fucoxanthin that provides the brown color of diatoms). The phenotype of the *alb3b* mutants pointed to a role of this protein in posttranslational insertion of FCPs into the thylakoid membrane. However, the ALB3b protein does not contain the basic Lys-rich C-terminal domain (CTD) known from plants to interact with other members of the CpSRP pathway (Falk *et al.*, 2010, Horn *et al.*, 2015, Chandrasekar and Shan, 2017). Instead, a CTD conserved within the group of diatoms was identified in the ALB3b insertase, but its protein interaction partners are unknown (Nymark *et al.*, 2019). ALB3a does contain the basic Lys-rich CTD, but repeated attempts to create knock out mutants of this insertase were unsuccessful, implying a crucial function in the co-translational CpSRP pathway similar to ALB3 and ALB3.2 of plants and green algae, respectively (Sundberg *et al.*, 1997, Göhre *et al.*, 2006, Nymark *et al.*, 2019).

Previously published experiments with *P. tricornutum cpsrp54* mutants indicated that loss of CpSRP54 causes increased high light sensitivity based on a more profound decrease in photosynthetic efficiency in mutants compared to WT when exposed to high intensity blue light (Nymark *et al.*, 2016). However, changes in the cell content of pigments and FCPs were not tested in mutant lines. Knowledge of the roles of members of the diatom CpSRP pathway is very limited, but based on currently available data CpSRP54 has been hypothesized to play a part in the co-translational part of the CpSRP pathway, but not in the post-translational part (Nymark *et al.*, 2016, Nymark *et al.*, 2019). To achieve further insight into the role of CpSRP54 in the CpSRP pathway, we investigated changes in photosynthetic properties, pigment level, protein abundance and growth characteristics as a response to light stress in *P. tricornutum cpsrp54* knockout (KO) lines. We propose a model illustrating the mechanistic differences of thylakoid protein insertion in diatoms, plants and green algae.

Results

Structural features of diatom CpSR54 proteins

The diatom CpSRP54 protein harbors the conserved multidomain structure of SRP54 proteins: A N-terminal helical bundle domain, a central SRP GTPase (G) domain and a methionine rich M-domain (Figure 1A). The N and G domains form a functional unit called the NG domain that is generally known to be necessary for binding and hydrolyzing GTP and interaction with a similar NG domain in its receptor, the FTSY protein (Pool, 2005, Ziehe *et al.*, 2017). The M-domain contains the conserved SRP RNA binding motif and is also responsible for interaction with ribosomes and signal sequences of cargo proteins (Pool, 2005, Chandrasekar and Shan, 2017, Ziehe *et al.*, 2017, Hristou *et al.*, 2019). In addition, the CpSRP54 contains a chloroplast targeting peptide (CTP). In plants, a conserved motif within the C-terminal region of the M-domain, ARRKR, is known to be important for CpSRP43 binding (Funke *et al.*, 2005, Dünschede *et al.*, 2015). This motif is poorly conserved in diatom CpSRP54 proteins and in CpSRP54 from *C. reinhardtii* which does not bind CpSRP43 (Figure 1D) (Dünschede *et al.*, 2015). These proteins contain a polybasic motif with two conserved arginines (the RR-motif in Figure 1A and D). The GTPase G1-G5 domains, the I-box, "ALL[DE]ADV", "D[SA]RGG", and "RILGMGD" motifs are all present in diatom CpSRP54 proteins. However, CpSRP54 proteins in diatoms have a 24 – 26 amino acid insertion between the G1 and G2 domain (Figure 1B). A model based on the crystal structure of *Arabidopsis thaliana* CpSRP54 and FTSY (PDB ID: 5L3R) using Swiss Model (Waterhouse *et al.*, 2018) suggests that this amino acid insert forms a loop-structure that does not directly interfere with the CpSRP54-FTSY interaction

surface (Figure 1C).

CRISPR/Cas9 editing of *CpSRP54* resulted in frame-shift mutations

Three CRISPR/Cas9 derived *cpsrp54* mutant lines (*cpsrp54-8*, *cpsrp54-11*, *cpsrp54-20*) originating from single cells from the M2, M4 and M8 lines, respectively (Nymark *et al.*, 2016) were selected for functional characterization. Frame-shift mutations were confirmed in all cell lines by TOPO cloning and subsequent Sanger sequencing of PCR products spanning the region targeted by the Cas9-gRNA complex. The Cas9/gRNA complex was designed to target a part of the *CpSRP54* gene (Phatr2_35185; XM_002179577) encoding the SRP54 N-terminal helical bundle domain of the CpSRP54 protein (Figure 1A). Polymorphisms in the *CpSRP54* gene confirmed that both alleles had been amplified and sequenced for *cpsrp54-8* and *cpsrp54-11* (Figure S1). Both *cpsrp54-8* and *cpsrp54-11* contained small indels. *Cpsrp54-20* contained a 212 bp insertion in one allele consisting of fragments from one of the vectors used for transformation of the *P. tricornutum* cells (Figure S1). The other allele of the *cpsrp54-20* line could not be amplified indicating larger insertions or deletion events preventing amplification by PCR. The frame-shift mutations caused premature stop codons shortly after the indels, resulting in truncated CpSRP54 proteins (Figure 1E).

Cpsrp54 mutants showed no visible coloration phenotype

The *alb3b* mutants displayed a distinct difference in coloration, lower absorbance in the blue-green part of the spectrum and a decreased transfer of energy from light harvesting antenna pigments Fx and Chl *c* to PSII compared to WT (Nymark *et al.*, 2019). If CpSRP54 functions in the same part of the CpSRP pathway as ALB3b, a similar phenotype would be expected. Cell culture color, *in vivo* fluorescence excitation and absorbance spectra from *cpsrp54* mutants and WT were therefore recorded. No visible color change could be seen in *P. tricornutum* *cpsrp54* mutants compared to WT that would indicate major differences in light harvesting antenna pigments content (Figure 2A). This observation was further supported by the close to identical *in vivo* fluorescence excitation and absorbance spectra from mutants and WT (Figure 2B-C). These results imply that the ability of mutants and WT to harvest light energy for photosynthesis as well as the different pigment's relative energy transfer efficiency to Chl *a* in the reaction center of PSII are identical (Figure 2B). The presented results are all from low light (LL, 35 umol photons m^{-2} s^{-1}) acclimated cells.

Cpsrp54 mutants are sensitive to increased light intensities

Based on the lack of a visible phenotype in LL and the indication that the *cpsrp54* mutants might be sensitive to increased light intensities (Nymark *et al.*, 2016), we decided to perform a more thorough investigation of pigment content and photophysiological responses of the *cpsrp54* mutants by exposing LL-acclimated cells (0 h) to medium light (ML, 200 µmol photons m^{-2} s^{-1}) intensities for 0.5, 6, 24, 48, and 168 h. Additionally, we calculated the stoichiometry of functional reaction centers, the photosynthetic electron flow and growth rates in LL and ML acclimated cells. As expected from the close to identical color and *in vivo* fluorescence excitation spectra, the pigment analyses confirmed that the content of Chl *a* and Fx in *cpsrp54* lines was similar to WT at most time points during the time series study (Figure 3A-B). In contrast, the conversion of the xanthophyll cycle pigment diadinoxanthin (Ddx) to the photoprotective pigment diatoxanthin (Dtx) was greatly enhanced in the mutants after the shift from LL to ML conditions as illustrated by the significantly higher Dtx content per cell (Figure 3D) and the elevated de-epoxidation state index (DES; DES = Dtx/(Dtx+Ddx); Figure 3E). Whereas the conversion of Ddx to Dtx peaked at the 0.5 h time point in the WT samples, the DES index reached its maximum after 6 h in ML in the *cpsrp54* lines and stayed at a higher level than WT during the entire length of the ML exposure experiment. In addition, the non-photochemical quenching (NPQ) capacity of the mutants was found to be 20-30% higher than that of the WT samples (Figure 3F). Altogether, these responses point towards a higher level of light stress in the mutants compared to the WT.

Chl *a* variable fluorescence measured with a pulse-amplitude modulated (PAM) fluorometer was used to monitor the physiological response of LL-acclimated *cpsrp54* KO mutants during acclimation to ML intensity. The photosynthetic (PSII) efficiency (F_v/F_m), the maximum light-utilization coefficient (the slope of the photosynthesis versus irradiance curves; α), the photosynthetic capacity (maximum relative electron transport rate, $rETR_{max}$) and the light saturation index ($E_k = rETR_{max}/\alpha$) were similar in *cpsrp54* and WT cultures in LL-acclimated cells (Figure 4A-D). Exposure to ML caused only a minor drop in F_v/F_m in WT cultures, whereas F_v/F_m was significantly lower in *cpsrp54* cultures compared to WT at all time points after the shift from LL to ML (Figure 4A). These results imply increased levels of photodamage and/or photoprotection when CpSRP54 is absent. The WT cells showed the expected response to increased light intensities displaying a pronounced increase in $rETR_{max}$ and E_k as a function of ML exposure time. In contrast, these values decreased or remained at LL levels in the *cpsrp54* cultures. The functional status of the photosynthetic apparatus of the *cpsrp54* mutants was compared to that of WT cells using the ElectroChromic Shift (ECS) signal. This is the

stark effect, i.e. a modification of the absorption properties of membrane embedded photosynthetic pigments following the buildup of a trans-thylakoid membrane potential during photosynthesis (Witt, 1979). The ECS signal can be used to determine spectroscopically the stoichiometry of functional reaction centers and the photosynthetic electron flow (Bailleul *et al.*, 2010). We used this approach to compare LL and ML-acclimated cells and found that the fraction of functional PSII reaction centers (RC) per functional PSI RC were less than half in the mutants compared to the WT in ML-acclimated cells, whereas no significant differences were found in LL-acclimated cells (Figure 4E). Similarly, the photosynthetic electron flow was around 50% lower in ML-grown *cpsrp54* lines than in WT cells (Figure 4F). The decreased photophysiological fitness of the *cpsrp54* mutants in ML is reflected also in an approx. 20% slower growth rate compared to WT at this light intensity (Table 1). The difference in growth rate did not increase further when the cells were grown in high light (HL; 1000 µmol photons m^{-2} s^{-1}).

Decreased rate of PSII repair

The increased susceptibility of the *cpsrp54* mutants to ML demonstrated above indicates an enhanced photosensitivity of the mutant strains, which could result from either an increased rate of photodamage to PSII core proteins or a decreased rate of PSII repair. To separate between these two phenomena, we performed an experiment where lincomycin (LINC), an inhibitor of chloroplast translation, was added to LL-acclimated cells before exposure to high light (HL; 1000 µmol photons m^{-2} s^{-1}) for 1 h. In parallel, cells without LINC were exposed to the same light treatment. Addition of LINC removes the possibility to synthesize new chloroplast proteins and PSII repair cannot take place. F_v/F_m was measured before the HL-treatment, after 1 h of HL, and after 30 min of recovery after the HL-treatment as an indicator of PSII functionality. The measurements performed directly after the 1 h HL treatment will be affected both by thermal dissipation of absorbed light energy (qE) and photodamaged PSII reaction centers (qI). 30 min of recovery in very dim light allows for relaxation of the rapidly reversible qE component of NPQ. No significant differences were found between LL-acclimated cultures or between cultures exposed to HL after addition of LINC (Figure 5). The HL+LINC combination caused a severe and close to identical decrease in F_v/F_m in WT and *cpsrp54* lines. An increase in F_v/F_m from ~25% to ~39 % of LL-levels was detected at the end of the 30 min dark period which can probably be attributed to relaxation of qE, although LINC might slow down the process (Bachmann *et al.*, 2004). Significant differences were found

between WT and *cpsrp54* lines in HL-treated cells without the addition of LINC (two-tailed Student's t-tests ($p<0.05$); Figure 5). After relaxation of qE, F_v/F_m recovered to 90% of the LL-levels in WT, whereas the equivalent average value in the *cpsrp54* cultures was ca. 70%. It is important to be aware that the use of the F_v/F_m to assess photodamage is liable to artefacts. Upon strong illumination, long living fluorescence quenching phenomena other than photodamage can contribute to change in fluorescence yield (Dall'Osto *et al.*, 2005). However, the fact that F_v/F_m recovers comparably in WT and mutants after LINC treatment (i.e. blocking PSII repair cycle; Figure 5) suggests that, if other long living quenching processes than photoinhibition were induced in our conditions, they were of the same extent in both genotypes. Our combined results are therefore interpreted to indicate that the rate of PSII repair is negatively affected by absence of CpSRP54, whereas the rate of PSII inactivation is highly similar.

Differences at the protein level

To investigate the effect of loss of CpSRP54 on the level of chloroplast proteins, quantitative proteomics of *cpsrp54-8* and *cpsrp54-11* cells that had been exposed to ML for 6 h was performed and compared to WT samples. The 6 h time point was chosen since the pigment and variable Chl fluorescence measurements described above indicated a high level of light stress at this timepoint in *cpsrp54* lines. Only proteins encoded in the chloroplast genome or predicted to contain chloroplast transit peptides sequences were chosen for analysis. Chloroplast proteins that were significantly regulated (FDR <0.01) in the same direction in both *cpsrp54* lines, showing $\log_2$ ratios $\geq \pm 0.5$ for at least one of the mutant lines and where at least two unique peptides were detected are included in Table 2. We further investigated the relative protein expression level of selected proteins by western blot. The most interesting findings are listed below.

Effects on the photosynthetic apparatus

Several FCPs involved in light harvesting were moderately affected in the *cpsrp54* mutant lines after 6 h of ML exposure, but the regulation was in most cases found to go in opposite direction in *cpsrp54-8* and *cpsrp54-11* compared to WT, meaning that none of these FCP proteins fulfilled the criteria for being included in Table 2. The significantly, but moderately, regulated FCP proteins were in general expressed at a lower level than WT in *cpsrp54-8* and at a higher level in *cpsrp54-11* (Supplementary Dataset 1). After 6 h in ML, the diatoms will be in the

process of downsizing their light harvesting antenna, and the results might reflect differences in acclimation status. Since the proteomics data recorded for the FCPs was inconclusive with regards to the effect of absence of CpSRP54, western blot analyses were additionally performed for a subgroup of FCPs, the LHCFs. The LHCF subgroup contains the major light-harvesting proteins in diatoms. The expression level of these proteins was investigated in total protein extracts from LL-acclimated cells, cells exposed to 6 h ML and ML-acclimated cells using an antibody predicted to detect LHCF1-11 (Figure 6A) (Juhas *et al.*, 2014). The observed differences in LHCF expression levels were very modest between mutants and WT, and additional blots were therefore produced from total protein extracts from LL and ML-acclimated cells. Relative abundances of LHCF proteins were estimated based on average ratios between *cpsrp54* and WT lines from several blots and two independent experiments (Figure S2). No differences in LHCF content was found between *crpsrp54* lines and WT in LL-acclimated cells, whereas prolonged growth in ML seemed to induce somewhat higher expression of LHCF proteins in the mutants than in WT (Figure 6B). These results are in line with the spectral properties (Figure 2) and light harvesting pigment data (Figure 3A-B) described above, indicating that loss of CpSRP54 does not result in a smaller light harvesting antenna in the *cpsrp54* lines.

Eleven chloroplast-encoded and one nucleus-encoded subunit of the photosynthetic electron transport (PET) chain complexes PSII, PSI, $Cytb_6f$ and ATPase fulfilled the above described criteria and were found to be moderately downregulated in the *cpsrp54* lines compared to WT after exposure to 6 h of ML (Table 2). Prolonged exposure to ML caused a decrease of the ratio of functional PSII/PSI in *cpsrp54* lines (Figure 4E). Light induced inactivation of PSII is typically caused by damage to the PSII RC core protein D1 (PsbA), but the proteomics data indicated that the lack of CpSRP54 had the strongest negative effect on the other PSII RC core protein D2 (PsbD; Table 2). D2 was among the strongest downregulated PET chain subunits, whereas D1 was only significantly downregulated in one of the mutant lines (Supplementary Dataset 1). To get a better overview of the content of PSII RC proteins in *cpsrp54* lines relative to WT, western blot analyses was performed on total protein extracts from LL-acclimated cells, cells exposed to 6 h ML and ML acclimated cells with antibodies specific to D1 and D2. The initial analysis of D1 and D2 supported a generally lower amount of D2 in the mutants compared to WT, whereas no clear effect on the relative abundance of D1 was observed at any light treatment (Figure 6A). As for the LHCF proteins relative quantification of D1 and D2 levels in LL and ML was performed running additional western blots (Figures S3-S4). Average

relative abundance values for D1 and D2 are presented in Figure 6C-D. The results indicated that D2 protein levels in *cpsrp54* mutants were lowered to around 70% of WT levels in both LL and ML conditions (Figure 6D). The relative content of D1 in mutants compared to WT showed larger variation between experiments, but was close to WT levels on average (Figure 6C; Figure S3). A negative effect of loss of CpSRP54 on the amount of D1 could therefore neither be proven from the proteomics nor the western blot analyses. In contrast to PSII core proteins, the subunits comprising the oxygen evolving complex (OEC) of PSII are mainly nucleus-encoded (except for PsbV). Of the OEC proteins detected by the proteomics data, PSBO, OEE3 and PsbV were unaffected by the loss of CpSRP54, whereas PSBP was slightly upregulated (Table 2). As for the PSII RC protein D1, the PSI RC proteins PsaA and PsaB were also only significantly downregulated in one of the lines, but the abundance of five other chloroplast-encoded PSI core subunits was found at lower levels in both mutant lines than in WT (Table 2; Supplementary Dataset 1). Two ferredoxin NAPD(H) reductases (FNRs), both nuclear-encoded, were among the strongest upregulated proteins in the dataset. FNR mainly catalyzes the final step in linear electron transport, reducing $NAPD^+$ to NADPH, but in plants some isoforms might also be involved in cyclic electron flow (CEF) around PSI, resulting in ATP formation (Goss and Hanke, 2014). However, the contribution of CEF in ATP production in diatoms is negligible (Bailleul *et al.*, 2015). The increased amount of FNR in *cpsrp54* mutants might be an attempt to compensate for the lower amounts of electrons available for NADPH formation in the mutants (Figure 4C and 4F).

Up-regulation of proteins connected to photoprotective responses

Several proteins known or predicted to be involved in photoprotective mechanisms were detected at moderately higher levels in mutants compared to WT (Table 2). LHCX1 and LHCX2 are FCP proteins important for NPQ and were upregulated in *cpsrp54* lines, consistent with the NPQ phenotype of the mutants (Figure 3F). A putative thylakoid bound ascorbate peroxidase (APX) likely to be involved in removal of H_2O_2 produced during photosynthesis was also expressed at higher levels in the mutants than in the WT. In addition, the expression of a protein annotated as a Cyclophilin type peptidyl-prolyl cis-trans isomerase was increased by around 50% in the mutants (Table 2). Chloroplast-localized cyclophilin type proteins has been found to be important for PSII biogenesis and repair in plants (Fu *et al.*, 2007, Järvi *et al.*, 2015).

Up-regulation of chaperones and possible interaction partners

Chloroplast-localized members of the four major families of ATP-dependent molecular

chaperones (chaperonin/Cpn60, Hsp70, Hsp90 and Hsp100 families) and cofactors were detected by the proteomics analyses. Of these, the chloroplast chaperon annotated as DnaK (Hsp70, chloroplast genome), its co-chaperone DNAJ (Hsp40) and the Hsp100 chaperone CLPB were expressed at higher levels in both the investigated mutant lines than in WT, with DnaK being the most upregulated chloroplast protein in our dataset (Table 2). The functions of these chaperons are unknown in diatoms, but HSP70 (DnaK homologs)- and HSP40 (DNAJ homologs)-type chaperons are known to be part of a network of molecular chaperons important for co-translational folding in chloroplasts (Ries *et al.*, 2020). In addition to protein folding, other proposed functions of stromal HSP70 chaperones include protein import into chloroplasts, protection/repair of PSII from photoinhibition and (dis-) assembly of vesicle-inducing protein in plastids 1 (VIPP1) oligomers (Trösch *et al.*, 2015). VIPP1 (also called the inner membrane-associated protein of 30 kDa (IM30)) proteins are highly conserved proteins found in cyanobacteria, algae and plants (Heidrich *et al.*, 2017, Siebenaller *et al.*, 2019). The exact function of VIPP1 is unclear, but it is proposed to be multifunctional and to be involved in thylakoid biogenesis/stabilization, coping with chloroplast membrane stress, remodeling of thylakoid membranes during light shifts and co-translational insertions of photosynthetic proteins (Walter *et al.*, 2015a, Heidrich *et al.*, 2017, Junglas and Schneider, 2018, Siebenaller *et al.*, 2019). The *P. tricornutum* homolog of VIPP1 was upregulated almost 2-fold in the *cpsrp54* mutants (Table 2). VIPP1 is known to dynamically shift between monomeric and oligomeric states, likely with the help of chaperons (Siebenaller *et al.*, 2019). DnaK-type chaperons and co-chaperones of the DNAJ type have been shown to interact with and impact the oligomeric state of VIPP1 in other photosynthetic organisms (Liu *et al.*, 2007, Gao *et al.*, 2015, Siebenaller *et al.*, 2019). CLPB belongs to the family of Caseinolytic proteases (CLP) that are important for removal of stress-related protein aggregates (Mishra and Grover, 2016). CLPB-type chaperones have been found to collaborate and directly interact with the DnaK system to solubilize and rescue aggregated proteins (Doyle *et al.*, 2015, Mogk *et al.*, 2015, Mishra and Grover, 2016).

Discussion

CpSRP54 is unlikely to play a role in post-translational targeting of FCPs to thylakoid membranes in diatoms

The role of CpSRP54 in the CpSRP pathway has previously been studied in the plant and green algal model organisms *A. thaliana* and *C. reinhardtii,* respectively (Amin *et al.*, 1999, Nilsson *et al.*, 1999, Hutin *et al.*, 2002, Nilsson and van Wijk, 2002, Rutschow *et al.*, 2008, Dünschede *et al.*, 2015, Walter *et al.*, 2015b, Jeong *et al.*, 2017, Hristou *et al.*, 2019). CpSRP54 targets members of the LHCP family to thylakoid membranes in both species through the post-translational pathway, and CpSRP54 KO mutants display a pale green color as a result of having a truncated light harvesting antenna (TLA) (Amin *et al.*, 1999, Hutin *et al.*, 2002, Rutschow *et al.*, 2008, Jeong *et al.*, 2017). In addition to the color change and the lower levels of antenna proteins and pigments, typical features of TLA mutants are increased photosynthetic activity per Chl and a higher light saturation point of photosynthesis (Kirst *et al.*, 2012a, Kirst *et al.*, 2012b, Kirst *et al.*, 2014, Jeong *et al.*, 2017). These features were all present in *P. tricornutum alb3b* mutants, and the TLA phenotype was interpreted as the ALB3b insertase playing an important, but not essential role in integration of FCPs into the thylakoid membrane in diatoms (Nymark *et al.*, 2019). In contrast, the *P. tricornutum cpsrp54* mutants did not display any of the above described TLA-features, and they displayed the WT phenotype for almost all measured parameters when grown in LL conditions. Taking into consideration also the CTD of the ALB3b insertase having unknown interaction partners and the absence of key players of the LHCP targeting machinery like the CpSRP43 chaperon and the LTD protein, an essential role for the diatom CpSRP54 in post-translational targeting of FCPs to thylakoid membranes seems highly unlikely. The post-translational part of the CpSRP pathway known to function in plants and green algae is the only SRP-mediated protein targeting process that is not a co-translational process (Pool, 2005, Ries *et al.*, 2020). It is tempting to speculate that the diatom CpSRP54 protein has not evolved to function post-translationally, and that an alternative strategy for targeting of FCPs to thylakoids exists in diatoms. However, a study performed by Lang and Kroth two decades ago showed that FCP integration into diatom thylakoid membranes is GTP-dependent (Lang and Kroth, 2001). They also showed that LHCPs from peas could be inserted into diatom thylakoids in the presences of GTP and diatom stromal extracts, and that diatom FCPs could be inserted into pea thylakoids under reciprocal experimental conditions, although to a lesser extent. In both experiments a low fraction of LHCPs/FCPs were seemingly also spontaneously integrated into thylakoids (Lang and Kroth, 2001).

At the time, the results were interpreted as LHCPs of plants and FCPs of diatoms being integrated through a highly similar CpSRP-dependent machinery. In light of the current knowledge of the CpSRP pathway in diatoms, another possible explanation for their results could be that the LHCPs and FCPs are similar enough to be recognized by two different thylakoid protein targeting machineries.

The phenotype of *cpsrp54* mutants indicates a role for the diatom CpSRP54 in the co-translational CpSRP pathway

Phenotypic differences are triggered by increased light intensities

One of the aims of this study was to test the hypothesis of CpSRP54 being involved in co-translational insertions of chloroplast encoded proteins into the thylakoid membrane. A shift from LL to ML conditions resulted in photophysiological differences between *cpsrp54* and WT that were in support of such a role. Despite stronger induction of photoprotective mechanisms (Figure 3D-F, Table 2) physiological parameters indicated higher levels of PSII inactivation in *cpsrp54* mutants compared to WT (Figure 4), likely to be caused by a moderately decreased rate of PSII repair (Figure 5). Similarly, a moderately reduced PSII repair efficiency has also been reported for *A. thaliana* mutants lacking CpSRP54 (Walter *et al.*, 2015b). Increased light intensities demand a higher rate of PSII repair involving an efficient removal and replacement of chloroplast encoded proteins prone to photodamage by a newly synthesized copy (Järvi *et al.*, 2015, Theis and Schroda, 2016). Loss of CpSRP54 might cause the replacement of damaged PSII core proteins to be less efficient. In plants, a connection between accumulation of non-functional PSII and down regulation of the activity and amount of zeaxanthin epoxidase (ZEP) has been shown (Bethmann *et al.*, 2019). ZEP is responsible for the reconversion of zeaxanthin to violaxanthin in plants and Ddx to Dtx in diatoms when the photosynthetic electron transport is no longer saturated either because of acclimation of the photosynthetic apparatus to higher light intensities or by transfer to low light conditions. If a connection between decreased ZEP amount/activity and increased PSII inhibition exists also in diatoms, it could explain the more limited back conversion of Dtx to Ddx in *cpsrp54* mutants after prolonged ML-treatment. NADPH is a cofactor of ZEP, and a slower epoxidation of Dtx to Ddx during acclimation to ML might also be caused by insufficient availability of NADPH because of the lower electron flow rate in the *cpsrp54* lines (Lavaud and Goss, 2014).

Physiological differences cannot be explained by changes in the abundance of PSII RC proteins

Analyses of the proteome after 6 h of ML exposure were performed hoping that this data could provide a molecular explanation for the light-induced phenotypic differences seen at the physiological level. A straightforward explanation for the increased level of photoinactivated PSII in *cpsrp54* lines would have been a decrease in the level of PSII RC proteins as a response to the light-treatment. Photosynthetic organisms typically display a high turnover rate of D1, and to a lesser extent D2, when subjected to increased light intensities (Aro *et al.*, 1993, Jansen *et al.*, 1996, Aro *et al.*, 2005, Rokka *et al.*, 2005). In contrast, marine diatom species are shown to have more similar turnover rates for D1 and D2 (Wu *et al.*, 2011, Wu *et al.*, 2012). The proteomics data confirmed a lower relative abundance of D2 in both the investigated *cpsrp54* lines, whereas the data for D1 was inconclusive. Additional analysis of D1 and D2 in cells acclimated to LL and ML detected roughly 30% lower levels of D2 in *cpsrp54* lines than in WT in both light conditions, whereas the relative amount of D1 varied between experiments, but was on average more similar to WT levels. The consistently lower amount of D2 found in all light treatments therefore seems to be a general feature of the *cpsrp54* mutants, and not a result of light stress. The photosynthetic performance of *cpsrp54* mutants is similar to WT levels in LL, meaning that there is no difference in functionality of the assembled PSII complexes in the mutants and WT, although the relative amount of one of the PSII core subunits seem to be lower. The existence of sub-pools of D1 and D2 that were not a part of active PSII has previously been reported for marine diatoms by Wu and coworkers (Wu *et al.*, 2011, Wu *et al.*, 2012). They also showed that a decrease in PSII activity often did not correlate with changes in D1 and D2 abundance (Wu *et al.*, 2012). A similar phenomenon seems likely in our study since the relative lower content of D2 compared to WT under the same light conditions is stable, whereas the difference in photosynthetic performance increases when shifted from LL to ML intensities. In support of our observations and previous reports is also a recent study of PSII supercomplexes in *P. tricornutum* thylakoid membranes, where a subpopulation of inactive/damaged PSII RCs not associated with FCP complexes was observed and suggested to function as PSII repair stations (Levitan *et al.*, 2019). The analysis of PSII RC proteins levels carried out in this study were performed on whole cell extracts and will not separate between proteins incorporated in functional PSIIs, proteins in inactivated PSIIs or unassembled D1 and D2 proteins.

Loss of *cpsrp54* triggers similar responses on the protein level in diatom and plants

In *A. thaliana*, there is convincing data supporting that CpSRP54 enhances the efficiency of co-translational insertion of a selection of chloroplast encoded subunits (Amin *et al.*, 1999, Nilsson *et al.*, 1999, Nilsson and van Wijk, 2002, Rutschow *et al.*, 2008, Piskozub *et al.*, 2015, Hristou *et al.*, 2019). Several studies have shown a reduced content of PSI and PSII RC proteins in developing *A. thaliana cpsrp54* mutants (Amin *et al.*, 1999, Rutschow *et al.*, 2008, Hristou *et al.*, 2019), and additional potential targets for CpSRP54 were revealed through a proteomic study, indicating that also other subunits of PSI, PSII and ATP synthase were negatively affected by a lack of CpSRP54 (Rutschow *et al.*, 2008). Direct evidence for the interaction of nascent chains of D1 of PSII and PetB of the $Cytb_6f$ complex with CpSRP54 also exists (Nilsson *et al.*, 1999, Nilsson and van Wijk, 2002, Piskozub *et al.*, 2015). A recent ribosome profiling study comparing thylakoid membrane association of translating ribosomes between WT and a mutant lacking CpSRP54 further confirmed CpSRP54's role in co-translational targeting of central photosynthetic proteins in plants (Hristou *et al.*, 2019). Similar to the results described above, several chloroplast-encoded subunits of PSI, PSII, $Cytb_6f$ and ATP synthase were found at moderately lower levels in the *P. tricornutum cpsrp54* mutants. In *A. thaliana*, the clearest effects of CpSRP54 depletion were seen on the level of PSI and PSII RC proteins, whereas in *P. tricornutum* only the PSII RC protein D2 was significantly downregulated in mutant lines. Despite some discrepancies in which subunits that were most severely affected by the loss of CpSRP54, and that we have no evidence for direct interaction between CpSRP54 and elongating thylakoid membrane proteins in *P. tricornutum*, the combined results from this study do imply that CpSRP54 is involved, but not essential, in targeting of chloroplast-encoded proteins to thylakoids in diatoms as well.

Effect of loss of CpSRP54 is alleviated by compensating mechanisms

The relatively mild phenotype of both the *A. thaliana* and *P. tricornutum cpsrp54* mutants might be partially explained by execution of compensation mechanisms involving the upregulation of chaperones that can alleviate the effects of loss of CpSRP54. Absence of CpSRP54 resulted in upregulation of DnaK homologs cpHSP70-1/2, CPN60 proteins, co-chaperonin CPN21 and ClpC-1/2 in *A. thaliana* (Rutschow *et al.*, 2008) and elevated levels of DnaK, DnaJ and ClpB in *P. tricornutum*. Upregulations of a range of cytoplasmic chaperons belonging mostly to the same families as the ones found in the chloroplastic responses, have also been reported as a common response to the loss of

cytoplasmic SRP54 in yeast and bacteria (Arnold and Wittrup, 1994, Mutka and Walter, 2001, Wickström *et al.*, 2011, Zhang *et al.*, 2012). Here, upregulation of the chaperone systems is believed to prevent the accumulation of mis-localized and aggregated proteins and might provide alternative pathways to target proteins to its target membranes (Arnold and Wittrup, 1994, Mutka and Walter, 2001, Wickström *et al.*, 2011, Zhang *et al.*, 2012). Although no functional data is available about roles and interaction partners of the chloroplast-localized DnaK in diatoms, the ~3-fold upregulation of the *P. tricornutum* DnaK in *cpsrp54* lines compared to WT suggests key roles for this multifunctional chaperon in coping with the stress of lacking CpSRP54. The simultaneous upregulation of DnaK, its putative cochaperone DnaJ and of one of their possible interaction partners, the diatom VIPP1 homolog, as a response to the lack of CpSRP54 opens for speculations about an indirect role of DnaK in insertion of thylakoid membrane proteins. As previously mentioned, the exact function of VIPP1 beyond its importance in thylakoid membrane biogenesis/maintenance is unclear, but one of its many suggested roles is connected to insertion of photosynthetic proteins (Bryan *et al.*, 2014, Trösch *et al.*, 2015, Heidrich *et al.*, 2017, Gutu *et al.*, 2018). In plants, VIPP1 has been detected as a component of D1 intermediates together with CpSRP54, CpFTSY, ALB3 and CpSecY, and found to stimulate insertion of D1 (Walter *et al.*, 2015a). Depletion of the ALB3.2 insertase of the co-translational CpSRP pathway in *C. reinhardtii* resulted in upregulation of VIPP1, the DnaK homolog HSP70B and its cochaperone (Göhre *et al.*, 2006). VIPP1 is also upregulated in *C. reinhardtti* mutants lacking the ALB3.1 insertase mainly involved in the posttranslational insertions of LHCPs, but absence of ALB3.1 also causes lower levels of D1 (Bellafiore *et al.*, 2002, Theis *et al.*, 2020). In addition, both HSP70B and VIPP1 are high light inducible and indicated to be involved in PSII repair in *C. reinhardtii* (Drzymalla *et al.*, 1996, Nordhues *et al.*, 2012, Trösch *et al.*, 2015). A possible connection between DnaK-type chaperones, VIPP1 and PS biogenesis has been suggested where the chaperones influence the activity of VIPP1 by catalyzing the assembly and disassembly of the VIPP1 oligomers, and where VIPP1 provides local areas where PS biogenesis can take place (Liu *et al.*, 2007, Rütgers and Schroda, 2013, Bryan *et al.*, 2014, Trösch *et al.*, 2015, Gutu *et al.*, 2018). A similar role in PS biogenesis for the DnaK-type chaperone system and VIPP1 in diatoms is imaginable, but no functional data is currently available to support such speculations.

Conclusion

Previous studies of the effects of loss of CpSRP54 in model organisms representing land plants and green microalgae and the current study of the effect of loss of CpSRP54 in the model diatom *P. tricornutum* show that although there are some similarities (see overview in Table 3), the mechanisms for targeting proteins to thylakoid membranes are too different for a direct transfer of knowledge from one group of species to another. A schematic representation of the CpSRP pathway for integration of thylakoid membrane proteins in *P. tricornutum* compared to plants (*A. thaliana*) and green algae (*C. reinhardtii*) is given in Figure 7. Major differences exist for the role of CpSRP54 in the three model systems. In *P. tricornutum* we suggest that CpSRP54, likely in interaction with the CpFTSY receptor, guides translating ribosomes to the ALB3a insertase (and possibly the CpSecY translocase) for co-translational insertion of chloroplast-encoded thylakoid membrane proteins (Figure 7A, right side) in a similar manner as the CpSRP54 of *A. thaliana* (Figure 7B, right side) (Ziehe *et al.*, 2018). *A. thaliana* CpSRP54 has a dual function and targets also LHCPs to thylakoid membranes (Figure 7B, left side). The role(s) of CpSRP54 in *P. tricornutum* and *A. thaliana* contrasts with the role of CpSRP54 in *C. reinhardtii*, which is reported to function exclusively in the post-translational insertion of LHCPs (Figure 7C, left side) (Jeong *et al.*, 2017). CpSRP54 and other members of the CpSRP pathway (CpFTSY and CpSRP43) have been suggested to be suitable universal targets for gene editing with the purpose of minimizing the chlorophyll antenna size in microalgae because of their role in the post-translational part of the CpSRP pathway in *C. reinhardtii* (Kirst and Melis, 2014, Jeong *et al.*, 2017). Truncation of the light harvesting antenna in green microalgae causes improved rates of growth and productivity under high-density and bright sunlight conditions, features that are desired from a commercial point of view (Kirst and Melis, 2014, Jeong *et al.*, 2017). The data presented above clearly show that such a phenotype is not achieved by disrupting the gene encoding CpSRP54 in *P. tricornutum*, and our data is only in support of a role for the CpSRP54 in the co-translational insertion of chloroplast-encoded proteins. Targeting of diatom FCP proteins to thylakoid membranes seems to be independent of the CpSRP pathway (Figure 7A, left side), making it unlikely that members of this pathway can be exploited in strain optimization for high density cultivation of diatoms.

Experimental procedures

The axenic *P. tricornutum* Bohlin clone Pt1 8.6 (CCMP632) culture was obtained from the culture collection of the Provasoli-Guillard National Center for Culture of Marine Phytoplankton, Bigelow Laboratory for Ocean Sciences, USA.

P. tricornutum cpsrp54 knock out mutants

The *cpsrp54-8*, *cpsrp54-11*, *cpsrp54-20* mutant lines used for this study were isolated from single cells from the M2, M4 and M8 lines, respectively, previously published in Nymark et al. (Nymark *et al.*, 2016). The *cpsrp54* KO mutants had been created with the aid of the CRISPR/Cas9 technology using a *P. tricornutum* culture derived from the sequenced clone Pt1 8.6 (Bowler *et al.*, 2008) as a starting point. Knock out mutations were confirmed in the three lines by TOPO cloning and subsequent Sanger sequencing of PCR products spanning the region of the *CpSRP54* gene targeted by the Cas9-gRNA complex as described previously (Nymark *et al.*, 2016, Nymark *et al.*, 2017)

Growth and experimental light conditions

P. tricornutum wild type (WT) cells and *cpsrp54* lines (*cpsrp54-8*, *cpsrp54-11*, *cpsrp54-20*) were cultured as described previously (Nymark *et al.*, 2009). Cell cultures were grown at 15°C under continuous cool white fluorescent light at scalar irradiance (E_{PAR}) of ~35 µmol photons m^{-2} s^{-1} (low light (LL)) or ~200 µmol photons m^{-2} s^{-1} (medium light (ML)), unless stated otherwise. High light (HL; ~1000 µmol photons m-2 s-1) was provided by a full spectrum LED lamp (5500 K). The cultures were kept in the exponential growth phase for at least two weeks under LL, ML or HL conditions before conducting experiments.

Growth rates

Growth rates were estimated in batch cultures of WT and *cpsrp54* KO lines (three biological replicates) acclimated to LL, ML or HL. The starting concentrations used for determining the growth rates were 200.000 cells/ml for LL-acclimated cells, 100.000 cells/ml for ML-acclimated cells and 50.000 cells/ml for HL-acclimated cells. Cells were fixed in Lugol's solution and counted by using a Bürker-Türk counting chamber or by flowcytometry as described previously (Nymark *et al.*, 2016). The average maximum growth rates (cell division/day) for WT and mutant lines were calculated by using the mean of the growth rates from the three biological replicates during the exponential phase.

In vivo fluorescence excitation

In vivo fluorescence excitation spectra were obtained from LL-acclimated WT and *cpsrp54* cultures (three biological replicates) using a Hitachi F-3000 spectrofluorometer (Hitachi Corp.) as previously described (Johnsen and Sakshaug, 2007, Nymark *et al.*, 2013). Excitation light was provided at 1 nm spectral resolution (5 nm bandwidth) from 400 to 700 nm, registering Chl *a* fluorescence emission at 730 nm (5 nm band width) as a function of absorbed light at the different wavelengths. 3-(3,4-dichlorophenyl)-1,1-dimethylurea (DCMU; 50 µM final concentration) was added 1 minute prior to each measurement to avoid variable fluorescence. All spectra were normalized to the red emission maximum of Chl *a* of the WT cultures.

Absorbance spectra

Absorption spectra were measured with a Multiscan sky spectrophotometer (Thermo Fisher Scientific, USA) with a resolution of 1 nanometer. Cells were loaded on a multiwell plate and spectra were normalized on the blue absorption peak. Data are representative of 3 biological replicates (3 technical replicates per genotype per experiment).

LL to ML shift time-series experiments

LL acclimated (0 h) *cpsrp54* KO lines were exposed to ML for 0.5, 6, 24, 48 h and 168 h. Three biological replicates were included for each line and time point. Cell concentrations were approx. 1 x 10^6 cells/mL at the day of harvesting. Harvested material was used for monitoring of the photophysiological state and pigment concentration per cell in LL and after the shift to ML. The time-series experiment in the current study and in a previously published study characterizing the *P. tricornutum alb3b* mutant (Nymark *et al.*, 2019) were performed in parallel and the responses of the *cpsrp54* and *alb3b* mutants were therefore compared to the same WT dataset.

Pigment analysis

Pigment analysis were performed by HPLC according to Rodriguez et al. (Rodriguez *et al.*, 2006) using a Hewlett-Packard HPLC 1100 Series system. Pigment values from the HPLC analysis were calculated as femtomol (fmol) pigment per cell. Cell concentrations were determined using a BD Accuri C6 Flow Cytometer as described previously (Nymark *et al.*, 2019).

Measurements of photosynthetic parameters

Variable *in vivo* Chl *a* fluorescence was measured as described in Nymark et al. (Nymark *et al.*, 2019) using a PhytoPAM (System I, Walz, Germany) equipped with a photomultiplier detector (PM-101P, Walz, Germany). The photosynthetic efficiency (F_v/F_m), the photosynthetic capacity (maximum relative electron transport rate ($rETR_{max}$), the maximum light utilization coefficient (α), the light saturation index ($E_k=rETR_{max}/\alpha$) and NPQ were calculated as described previously (Nymark *et al.*, 2009, Nymark *et al.*, 2019). NPQ data was derived from light response curves from LL-acclimated cultures. All samples were incubated 3 min in darkness prior to performing measurements. A Peltier cell (US-T/S, Walz) kept the temperature at 15°C (±0.2°C) during the measurements.

The ECS signal in LL and ML-acclimated cells was measured with a Joliot-type spectrophotometer (JTS-10, Biologic) equipped with a laser or xenon lamp as excitation sources, white probing light and interference filters (3-8 nm bandwidth) allowing measurements of the absorption difference signals at selected wavelengths (Bailleul *et al.*, 2015). All cultures were upconcentrated to 20 million cells/ml by centrifugation prior to performing the measurements. Measurements of PSII/PSI stoichiometries were measured under single turnover flash regime. ECS kinetics were triggered by excitation with a saturating light flash produced by a laser or xenon lamp causing a single charge separation in all active PSs. Three different phases were observed: a fast rise of the signal corresponding to charge separation in PSI and PSII (<100 µs after laser flash), a slower rise (ms time range) representing electron flow through $Cytb_6f$ and a decay phase due to charge leakage through the membrane (Bailleul *et al.*, 2010). The linear component of the ECS (ECS_{lin}) was used to estimate the PSII/PSI ratio. ECS_{lin} was deconvoluted from superimposed signals by measuring at three different wavelengths (520, 554 and 563 nm) as described in Bailleul et al. (Bailleul *et al.*, 2015). Briefly, we first assessed the contribution of c-type cytochromes in the measured signal as Cyt c= [554] – 0.4 x [520] – 0.4 x [563], where [554], [520] and [566] were the measured absorption difference signals at the three different wavelengths. Secondly, we evaluated ECS_{lin} as = [520] – 0.25 x Cyt c. PSII contribution was evaluated from the amplitude of the fast ECS_{lin} phase as the decrease in the signal amplitude upon poisoning samples with DCMU (20µM) and hydroxylamine (HA; 1 mM) to irreversibly block PSII charge separation. PSI was estimated as the fraction of the signal that was insensitive to these inhibitors (Bailleul *et al.*, 2010).

The same approach was used to evaluate photosynthetic electron flow (electrons per second) in LL

and ML-acclimated WT and *cpsrp54* cells. Cells were illuminated with continuous red light (590 µmol photons m^{-2} s^{-1}) until steady state photosynthesis was achieved. Then, light was switched off and the rate of photosynthetic electron flow was measured as described in (Bailleul *et al.*, 2010). Briefly, in steady state the ECS signal reflects membrane potential generation by the PSs and $Cytb_6f$ complex and membrane potential dissipation by the ATP synthase. When light is switched off, PSII and PSI activity stops abruptly, while ATP synthase and the $Cytb_6f$ complex activities remain (transiently) unchanged. Therefore, the difference between the slopes of the ECS signal measured in the light and after the light is switched off is proportional to the rate of PSI and PSII photochemistry (i.e. to the rate of electron flow). This rate can be quantified by dividing the slope difference by the amplitude of the fast ECS_{lin} phase measured under single turnover flashes in the presence of DCMU and HA. The latter reflects the ECS absorption changes induced by the transfer of a single charge across the membrane (e.g. one electron per photosynthetic chain).

High light lincomycin experiment

Lincomycin (LINC; Sigma-Aldrich) blocks chloroplast protein synthesis (Ridley and Ridley, 1979) and was added to LL-acclimated cultures (3 biological replicates) in the exponential phase at a final concentration of 500 µg mL^{-1}. Cultures were incubated in darkness for 15 min before exposure to HL (1000 µmol photons m^{-2} s^{-1}) for 1 h. In parallel, cultures without LINC were exposed to the same treatment. F_v/F_m was measured in LL and HL treated cultures using an AquaPen-C (Photon System Instruments). LL acclimated cells were incubated in darkness for 3 min prior to measurements, whereas HL-treated cells were measured after both a 3 min and 30 min very dim light period. The additional measurement after 30 min was included to relax the rapidly reversible qE component of NPQ so that only the photoinihibitory, slowly reversible quenching (qI), caused by damaged PSII reaction centers, would influence the F_v/F_m value.

Proteomics

Proteomic analyses were performed of *cpsrp54-8*, *cpsrp54-11* and WT lines after 6 h exposure to ML. Five biological replicates were included for each line, and cells were harvested by filtration as described previously (Nymark *et al.*, 2019). To each sample, 100 µl of SDC buffer (1% SDC, 10 mM TCEP, 40 mM 2-Chloroacetamide, Roche Protease Inhibitor cocktail, 100 mM Tris pH 8.5) was added. After mixing by pipetting, contents were transferred to LoBind tubes (Eppendorf), the tubes were kept at 95 °C for 5 minutes, before being sonicated at 4 °C in a Bioruptor Pico (Diagenode) for

10 cycles, each with 1 min sonication followed by 30 sec without sonication. Protein concentration was measured in a Direct Detect (Millipore) and a volume containing 50 µg total protein was separated for further sample preparation. The volume was adjusted to 50 µl by addition of water. Next, a KingFisher Flex (Thermo Scientific) magnetic-bead handling robot performed clean-up of the proteins using HILIC magnetic microparticles (ReSyn Bioscience) followed by tryptic digestion into peptides. In more details, deep well plates were prepared and placed into the KingFisher as: 25 µl of HILIC microparticles (20 mg/ml) and 175 µl Equilibration buffer (15% Acetonitrile, 100 mM Ammonium acetate pH 4.5) at position 1, 500 µl Equilibration buffer at position 2, 50 µl sample and 50 µl Bind buffer (0.5% SDS, 30% Acetonitrile, 200 mM Ammonium acetate pH 4.5) at position 3, 200 µl 95% Acetonitrile at positions 4 and 5, 50 µl Trypsin (0.1 µg/µl in 45 mM Acetic Acid) and 150 µl Digestion buffer (20 mM Ammonium formate pH 8.2) at position 6, comb Tip at position 7. Then the robot executed the following protocol: picked up the comb tip, collected HILIC magnetic particles, equilibrated HILIC magnetic particles in Equilibration buffer, bound protein to HILIC magnetic particles, washed in high organic content twice, eluted from HILIC and digested protein with Trypsin at 37° for 4 hours, removed HILIC magnetic particles. BindIt Software 3.3.1 (Thermo Scientific) was used to prepare the robot protocol and to run it. Unless otherwise-stated, chemicals were from Sigma.

Subsequently the digested peptides were transferred to new tubes, they were acidified by addition of 2 µl formic acid, then the tubes were spun-down (16,000g for 5 min) and 100 µl of supernatants were transferred to LC-MS vials. Analysis was performed on an EASY-nLC 1200 UHPLC system (Thermo Scientific) interfaced with an Q Exactive HF mass spectrometer (Thermo Scientific) via a Nanospray Flex ion source (Thermo Scientific). Peptides were injected onto an Acclaim PepMap100 C18 trap column (75 µm i.d., 2 cm long, 3 µm, 100 Å, Thermo Scientific) and further separated on an Acclaim PepMap100 C18 analytical column (75 µm i.d., 50 cm long, 2 µm, 100 Å, Thermo Scientific) at 250 nl/min using a 180-minute gradient (145 min 5%-35% B, 15 min 35%-100% B, 20 min 100% B; where A is 0.1 % formic acid and B is 0.1 % formic acid, 80% acetonitrile). Unless otherwise-stated, chemicals were from Fisher Scientific.

Peptide ions were analysed in positive ion mode under data dependent acquisition using the following parameters: Electrospray voltage 1.9 kV, HCD fragmentation with normalized collision energy 27. Each MS scan (200 to 2000 m/z, 3e6 AGC target, profile) was acquired at a resolution of 60,000 FWHM, followed by 15,000 FWHM MS/MS scans (200 to 2000 m/z, 1.2 m/z isolation width, 1e5

AGC target, 48 ms maximum IT, centroid) triggered for the 15 most intense ions, with a 25 s dynamic exclusion. Charge exclusion was set to unassigned, 1 and greater than 5.

Proteins were identified and quantified by processing the MS data using Thermo Scientific Proteome Discoverer (Thermo Scientific) version 2.3/4. Preview version 2.3.5 from Protein Metrics Incorporated (Kil *et al.*, 2011) was used to inspect the raw files to determine optimal search criteria. Namely, following search parameters were used: enzyme specified as Trypsin with maximum two missed cleavages allowed; Acetylation of Protein N-terminal with Met-loss (Bonissone *et al.*, 2013), Oxidation of Methionine and Deamidation of Asparagine/Glutamine as dynamic post-translational modification while Carbamidomethylation of Cysteine as static; Precursor mass-tolerance of 20 PPM while Fragment mass-tolerance of 0.02 Dalton. Spectrum file RC, PD's node, was set up to query the raw files against the *Phaeodactylum tricornutum* (strain CCAP 1055/1) downloaded from Uniprot (https://www.uniprot.org/proteomes/UP000000759) in December 2018 and internal contaminants database to recalibrate and detect features with the Minora node and Sequest (Eng *et al.*, 1994) search engines available PD. For downstream analysis of these peptide-spectra-matches (PSM), both protein and peptide identifications/PSM false-discovery-rate (FDR) was set to 1% as high and 5% as medium confidence, thus only unique peptides with these confidences thresholds were used for final protein group identification and label the level of confidence respectively. Each protein group abundance was normalized by the total abundance of all identified peptides/PSM at the FDR mentioned earlier and scaled on all average with Precursor Ion Quantifier node of PD.

Protein isolation, SDS-PAGE and Western blot analysis

Cell harvesting, total protein isolation, determination of protein concentration, SDS-PAGE and Western blot analysis were performed as previously described (Nymark *et al.*, 2019) using material from WT and *cpsrp54* cultures acclimated to either LL or ML. Proteins were detected with the following antibodies: anti-D1 (AS05 084 Agrisera; 1:20000 dilution), anti-D2 (AS06 146 Agrisera; 1:5000), anti-AtpB (AS05 085, Agrisera; 1:4000) and anti-LHCF1-11 (1:1000) (kind gift from C. Büchel, University of Frankfurt, Germany; (Juhas *et al.*, 2014). Primary antibody incubation was performed overnight at 4°C for all antibodies. Secondary antibody incubation was performed for 2 h at room temperature using Goat anti-Rabbit IgG (H+L) Secondary Antibody, HRP conjugate (ThermoFisher, 1:10000). Proteins were detected with SuperSignal West Pico PLUS Chemiluminescent Substrate (Thermo Scientific) and the blots were imaged using a G:BOX ChemiXRQ gel doc system (Syngene).

Statistical analysis

The R package ROTS (reproducibility-optimized test statistic) was used for statistical analysis of the proteomics data aiming to identify differentially expressed proteins in *cpsrp54-8* and *cpsrp54-11* compared to WT after 6 h exposure to ML (Suomi *et al.*, 2017). ROTS employs a bootstrapping method to identify the proper t-test statistics based on the data. Prior to the differential expression analysis, the intensity counts were normalized across samples. Additionally, for the validity of the results, the homogeneity in pair-wise and group-wise variances was tested using an F-test and a p-value of 0.05 as a significance threshold. Once normality and homogeneity in variance were ensured, two independent tests were performed; one for WT against *cpsrp54-8* and one for WT against *cpsrp54-11*. The differential expression analysis was performed using $\log_2$ transformed values, while proteins with only one abundance value across the samples were omitted. For both tests, the number of bootstrapping and the number of top-ranked features for reproducibility optimization were set to 1000.

Two-way ANOVA with Dunnet's multiple comparison tests were carried out using GraphPad Prism Software (version 8.4.3) to determine if there were significant differences ($p<0.05$) between the pigment levels and photosynthetic parameters in *cpsrp54* mutants compared to WT.

Accession numbers

The CpSRP54 gene has Draft ID Phatr2_35185 and NCBI accession number XM_002179577. UniProt accession numbers for differentially expressed proteins discussed in the text are included in Table 2. UniProt accession numbers are provided for all proteins detected by the proteomics analyses and the data are deposited to the ProteomeXchange Consortium as described below in the Data availability statement.

Data availability statement

A complete submission of proteomics data including raw data (raw), peak-list (mzML), identifications (mzID), workflow (pdAnalysis) and annotated results (xlsx) has been deposited to the ProteomeXchange Consortium via the PRIDE (Perez-Riverol *et al.*, 2019) partner repository with the dataset identifier PXD020167 and 10.6019/PXD020167. All other relevant information can be found within the manuscript and its supporting information.

Acknowledgements

We wish to thank Kjersti Andresen for assistance with the HPLC analyses and Professor Claudia

Büchel for kindly providing LHCF antibodies. The authors would also like to thank Stoyan Stoychev at ReSyn Bioscience for helpful discussions on the HILIC sample preparation protocol, and Felicity Ashcroft for help with statistical analyses.

Author contributions

M.N., P.W. and A.M.B. conceived the research plans. M.N., P.W. and G.F. supervised and designed the experiments. M.N., M.C.G.H., C.V., D.M.F., M.S. and G.F. performed the experiments. M.N., M.C.G.H., C.V., D.M.F., A.S., E.T., P.W. and G.F. analyzed the data. M.N. wrote the article with contributions from co-authors. M.N. agrees to serve as the author responsible for contact and ensures communication.

Funding

This work was supported by a grant from the Research Council of Norway to A.M.B through funding of the project "Downsizing light harvesting antennae to scale up production potential and valorization from cultivation of marine microalgae" (project no. 267474), to Olav Vadstein through funding of the project Microbially Produced Raw Materials for Aquafeed (project no. 239001) and the NTNU enabling technologies program to P.W.

Conflict of interest

The authors declare that they have no competing interests.

Supporting information

Figure S1. DNA sequence alignments of the *cpsrp54* mutant lines.

Figure S2. Overview of blots used for calculations of LHCF1-11 protein expression levels in WT and *cpsrp54* lines acclimated to LL and ML.

Figure S3. Overview of blots used for calculations of D1 protein expression levels in WT and *cpsrp54* lines grown in LL or ML.

Figure S4. Overview of blots used for calculations of D2 protein expression levels in WT and *cpsrp54* lines grown in LL or ML.

Supplementary Dataset 1. Significantly regulated proteins comprising the photosynthetic apparatus.

References

Amin, P., Sy, D.A., Pilgrim, M.L., Parry, D.H., Nussaume, L. and Hoffman, N.E. (1999) Arabidopsis mutants lacking the 43- and 54-kilodalton subunits of the chloroplast signal recognition particle have distinct phenotypes. *Plant Physiol*, **121**, 61-70. https://doi.org/10.1104/pp.121.1.61

Armbrust, E.V. (2009) The life of diatoms in the world's oceans. *Nature*, **459**, 185-192. https://doi.org/10.1038/nature08057

Arnold, C.E. and Wittrup, K.D. (1994) The stress response to loss of signal recognition particle function in *Saccharomyces cerevisiae*. *J Biol Chem*, **269**, 30412-30418

Aro, E.M., Suorsa, M., Rokka, A., Allahverdiyeva, Y., Paakkarinen, V., Saleem, A., Battchikova, N. and Rintamaki, E. (2005) Dynamics of photosystem II: a proteomic approach to thylakoid protein complexes. *J Exp Bot*, **56**, 347-356. https://doi.org/10.1093/jxb/eri041

Aro, E.M., Virgin, I. and Andersson, B. (1993) Photoinhibition of Photosystem II. Inactivation, protein damage and turnover. *Biochim Biophys Acta*, **1143**, 113-134. https://doi.org/10.1016/0005-2728(93)90134-2

Bachmann, K.M., Ebbert, V., Adams, W.W., Verhoeven, A.S., Logan, B.A. and Demmig-Adams, B. (2004) Effects of lincomycin on PSII efficiency, non-photochemical quenching, D1 protein and xanthophyll cycle during photoinhibition and recovery. *Funct Plant Biol*, **31**, 803-813. https://doi.org/10.1071/Fp04022

Bailleul, B., Berne, N., Murik, O., Petroutsos, D., Prihoda, J., Tanaka, A., Villanova, V., Bligny, R., Flori, S., Falconet, D., Krieger-Liszkay, A., Santabarbara, S., Rappaport, F., Joliot, P., Tirichine, L., Falkowski, P.G., Cardol, P., Bowler, C. and Finazzi, G. (2015) Energetic coupling between plastids and mitochondria drives CO_2 assimilation in diatoms. *Nature*, **524**, 366-369. https://doi.org/10.1038/nature14599

Bailleul, B., Cardol, P., Breyton, C. and Finazzi, G. (2010) Electrochromism: a useful probe to study algal photosynthesis. *Photosynth Res*, **106**, 179-189. https://doi.org/10.1007/s11120-010-9579-z

Bellafiore, S., Ferris, P., Naver, H., Gohre, V. and Rochaix, J.D. (2002) Loss of Albino3 leads to the specific depletion of the light-harvesting system. *Plant Cell*, **14**, 2303-2314

Bethmann, S., Melzer, M., Schwarz, N. and Jahns, P. (2019) The zeaxanthin epoxidase is degraded along with the D1 protein during photoinhibition of photosystem II. *Plant Direct*, **3**. https://doi.org/10.1002/pld3.185

Bonissone, S., Gupta, N., Romine, M., Bradshaw, R.A. and Pevzner, P.A. (2013) N-terminal protein processing: a comparative proteogenomic analysis. *Mol Cell Proteomics*, **12**, 14-28. https://doi.org/10.1074/mcp.M112.019075

Bowler, C., Allen, A.E., Badger, J.H., Grimwood, J., Jabbari, K., Kuo, A., Maheswari, U., Martens, C., Maumus, F., Otillar, R.P., Rayko, E., Salamov, A., Vandepoele, K., Beszteri, B., Gruber, A., Heijde, M., Katinka, M., Mock, T., Valentin, K., Verret, F., Berges, J.A., Brownlee, C., Cadoret, J.P., Chiovitti, A., Choi, C.J., Coesel, S., De Martino, A., Detter, J.C., Durkin, C., Falciatore, A., Fournet, J., Haruta, M., Huysman, M.J., Jenkins, B.D., Jiroutova, K., Jorgensen, R.E., Joubert, Y., Kaplan, A., Kroger, N., Kroth, P.G., La Roche, J., Lindquist, E., Lommer, M., Martin-Jezequel, V., Lopez, P.J., Lucas, S., Mangogna, M., McGinnis, K., Medlin, L.K., Montsant, A., Oudot-Le Secq, M.P., Napoli, C., Obornik, M., Parker, M.S., Petit, J.L., Porcel, B.M., Poulsen, N., Robison, M., Rychlewski, L., Rynearson, T.A., Schmutz, J., Shapiro, H., Siaut, M.,

Stanley, M., Sussman, M.R., Taylor, A.R., Vardi, A., von Dassow, P., Vyverman, W., Willis, A., Wyrwicz, L.S., Rokhsar, D.S., Weissenbach, J., Armbrust, E.V., Green, B.R., Van de Peer, Y. and Grigoriev, I.V. (2008) The *Phaeodactylum* genome reveals the evolutionary history of diatom genomes. *Nature*, **456**, 239-244. https://doi.org/10.1038/nature07410

Bozarth, A., Maier, U.G. and Zauner, S. (2009) Diatoms in biotechnology: modern tools and applications. *Appl Microbiol Biotechnol*, **82**, 195-201. https://doi.org/10.1007/s00253-008-1804-8

Brembu, T., Winge, P., Tooming-Klunderud, A., Nederbragt, A.J., Jakobsen, K.S. and Bones, A.M. (2014) The chloroplast genome of the diatom Seminavis robusta: new features introduced through multiple mechanisms of horizontal gene transfer. *Mar Genomics*, **16**, 17-27. https://doi.org/10.1016/j.margen.2013.12.002

Bryan, S.J., Burroughs, N.J., Shevela, D., Yu, J., Rupprecht, E., Liu, L.N., Mastroianni, G., Xue, Q., Llorente-Garcia, I., Leake, M.C., Eichacker, L.A., Schneider, D., Nixon, P.J. and Mullineaux, C.W. (2014) Localisation and interactions of the Vipp1 protein in cyanobacteria. *Mol Microbiol*. https://doi.org/10.1111/mmi.12826

Butler, T., Kapoore, R.V. and Vaidyanathan, S. (2020) *Phaeodactylum tricornutum*: A diatom cell factory. *Trends Biotechnol*, **38**, 606-622. https://doi.org/10.1016/j.tibtech.2019.12.023

Chandrasekar, S. and Shan, S.O. (2017) Anionic phospholipids and the Albino3 translocase activate signal recognition particle-receptor interaction during light-harvesting chlorophyll *a/b*-binding protein targeting. *J Biol Chem*, **292**, 397-406. https://doi.org/10.1074/jbc.M116.752956

Dall'Osto, L., Caffarri, S. and Bassi, R. (2005) A mechanism of nonphotochemical energy dissipation, independent from PsbS, revealed by a conformational change in the antenna protein CP26. *Plant Cell*, **17**, 1217-1232. https://doi.org/10.1105/tpc.104.030601

Dittami, S.M., Michel, G., Collen, J., Boyen, C. and Tonon, T. (2010) Chlorophyll-binding proteins revisited-a multigenic family of light-harvesting and stress proteins from a brown algal perspective. *BMC Evol Biol*, **10**, 365. https://doi.org/10.1186/1471-2148-10-365

Doyle, S.M., Shastry, S., Kravats, A.N., Shih, Y.H., Miot, M., Hoskins, J.R., Stan, G. and Wickner, S. (2015) Interplay between E. coli DnaK, ClpB and GrpE during protein disaggregation. *J Mol Biol*, **427**, 312-327. https://doi.org/10.1016/j.jmb.2014.10.013

Drzymalla, C., Schroda, M. and Beck, C.F. (1996) Light-inducible gene HSP70B encodes a chloroplast-localized heat shock protein in *Chlamydomonas reinhardtii*. *Plant Mol Biol*, **31**, 1185-1194. https://doi.org/10.1007/BF00040835

Dünschede, B., Träger, C., Schröder, C.V., Ziehe, D., Walter, B., Funke, S., Hofmann, E. and Schünemann, D. (2015) Chloroplast SRP54 was recruited for posttranslational protein transport via complex formation with chloroplast SRP43 during land plant evolution. *J Biol Chem*, **290**, 13104-13114. https://doi.org/10.1074/jbc.M114.597922

Eng, J.K., McCormack, A.L. and Yates, J.R. (1994) An approach to correlate tandem mass spectral data of peptides with amino acid sequences in a protein database. *J Am Soc Mass Spectrom*, **5**, 976-989. https://doi.org/10.1016/1044-0305(94)80016-2

Falk, S., Ravaud, S., Koch, J. and Sinning, I. (2010) The C terminus of the Alb3 membrane insertase recruits cpSRP43 to the thylakoid membrane. *J Biol Chem*, **285**, 5954-5962. https://doi.org/10.1074/jbc.M109.084996

Flori, S., Jouneau, P.H., Finazzi, G., Marechal, E. and Falconet, D. (2016) Ultrastructure of the periplastidial compartment of the diatom *Phaeodactylum tricornutum*. *Protist*, **167**, 254-267. https://doi.org/10.1016/j.protis.2016.04.001

Fu, A., He, Z.Y., Cho, H.S., Lima, A., Buchanan, B.B. and Luan, S. (2007) A chloroplast cyclophilin and maintenance of functions in the assembly photosystem II in *Arabidopsis thaliana*. *P Natl Acad Sci USA*, **104**, 15947-15952. https://doi.org/10.1073/pnas.0707851104

Funke, S., Knechten, T., Ollesch, J. and Schünemann, D. (2005) A unique sequence motif in the 54-kDa subunit of the chloroplast signal recognition particle mediates binding to the 43-kDa subunit. *J Biol Chem*, **280**, 8912-8917. https://doi.org/10.1074/jbc.M409992200

Gao, F., Wang, W.Y., Zhang, W.J. and Liu, C.M. (2015) α-helical domains affecting the oligomerization of Vipp1 and its interaction with Hsp70/DnaK in *Chlamydomonas*. *Biochemistry*, **54**, 4877-4889. https://doi.org/10.1021/acs.biochem.5b00050

Gibbs, S.P. (1970) Comparative ultrastructure of algal chloroplast. *Ann Ny Acad Sci*, **175**, 454-+. https://doi.org/10.1111/j.1749-6632.1970.tb45167.x

Gibbs, S.P. (1981) The chloroplasts of some algal groups may have evolved from endosymbiotic eukaryotic algae. *Ann Ny Acad Sci*, **361**, 193-208. https://doi.org/ 10.1111/j.1749-6632.1981.tb46519.x

Gilbert, J.A., Field, D., Swift, P., Newbold, L., Oliver, A., Smyth, T., Somerfield, P.J., Huse, S. and Joint, I. (2009) The seasonal structure of microbial communities in the Western English Channel. *Environ Microbiol*, **11**, 3132-3139. https://doi.org/10.1111/j.1462-2920.2009.02017.x

Goss, T. and Hanke, G. (2014) The end of the line: Can ferredoxin and ferredoxin NADP(H) oxidoreductase determine the fate of photosynthetic electrons? *Curr Protein Pept Sc*, **15**, 385-393. https://doi.org/10.2174/1389203715666140327113733

Grossman, A.R., Bhaya, D., Apt, K.E. and Kehoe, D.M. (1995) Light-harvesting complexes in oxygenic photosynthesis: diversity, control, and evolution. *Annu Rev Genet*, **29**, 231-288. https://doi.org/10.1146/annurev.ge.29.120195.001311

Grouneva, I., Gollan, P.J., Kangasjarvi, S., Suorsa, M., Tikkanen, M. and Aro, E.M. (2013) Phylogenetic viewpoints on regulation of light harvesting and electron transport in eukaryotic photosynthetic organisms. *Planta*, **237**, 399-412. https://doi.org/10.1007/s00425-012-1744-5

Gutu, A., Chang, F. and O'Shea, E.K. (2018) Dynamical localization of a thylakoid membrane binding protein is required for acquisition of photosynthetic competency. *Mol Microbiol*, **108**, 16-31. https://doi.org/10.1111/mmi.13912

Göhre, V., Ossenbuhl, F., Crevecoeur, M., Eichacker, L.A. and Rochaix, J.D. (2006) One of two Alb3 proteins is essential for the assembly of the photosystems and for cell survival in *Chlamydomonas*. *Plant Cell*, **18**, 1454-1466. https://doi.org/10.1105/tpc.105.038695

Heidrich, J., Thurotte, A. and Schneider, D. (2017) Specific interaction of IM30/Vipp1 with cyanobacterial and chloroplast membranes results in membrane remodeling and eventually in membrane fusion. *Bba-Biomembranes*, **1859**, 537-549. https://doi.org/10.1016/j.bbamem.2016.09.025

Hohmann-Marriott, M.F. and Blankenship, R.E. (2011) Evolution of photosynthesis. *Annu Rev Plant Biol*, **62**, 515-548. https://doi.org/10.1146/annurev-arplant-042110-103811

Horn, A., Hennig, J., Ahmed, Y.L., Stier, G., Wild, K., Sattler, M. and Sinning, I. (2015) Structural basis for cpSRP43 chromodomain selectivity and dynamics in Alb3 insertase interaction. *Nat Commun*, **6**, 8875. https://doi.org/10.1038/ncomms9875

Hristou, A., Gerlach, I., Stolle, D.S., Neumann, J., Bischoff, A., Dunschede, B., Nowaczyk, M.M., Zoschke, R. and Schunemann, D. (2019) Ribosome-associated chloroplast SRP54 enables efficient cotranslational membrane insertion of key photosynthetic proteins. *Plant Cell*, **31**, 2734-2750. https://doi.org/10.1105/tpc.19.00169

Hutin, C., Havaux, M., Carde, J.P., Kloppstech, K., Meiherhoff, K., Hoffman, N. and

Nussaume, L. (2002) Double mutation cpSRP43^{-}/cpSRP54^{-} is necessary to abolish the cpSRP pathway required for thylakoid targeting of the light-harvesting chlorophyll proteins. *Plant J*, **29**, 531-543. https://doi.org/10.1046/j.0960-7412.2001.01211.x

Jansen, M.A.K., Greenberg, B.M., Edelman, M., Mattoo, A.K. and Gaba, V. (1996) Accelerated degradation of the D2 protein of photosystem II under ultraviolet radiation. *Photochem Photobiol*, **63**, 814-817. https://doi.org/10.1111/j.1751-1097.1996.tb09636.x

Jeong, J., Baek, K., Kirst, H., Melis, A. and Jin, E. (2017) Loss of CpSRP54 function leads to a truncated light-harvesting antenna size in *Chlamydomonas reinhardtii*. *Biochim Biophys Acta Bioenerg*, **1858**, 45-55. https://doi.org/10.1016/j.bbabio.2016.10.007

Jeong, J., Baek, K., Yu, J., Kirst, H., Betterle, N., Shin, W., Bae, S., Melis, A. and Jin, E. (2018) Deletion of the chloroplast LTD protein impedes LHCI import and PSI-LHCI assembly in *Chlamydomonas reinhardtii*. *J Exp Bot*, **69**, 1147-1158. https://doi.org/10.1093/jxb/erx457

Johnsen, G. and Sakshaug, E. (2007) Biooptical characteristics of PSII and PSI in 33 species (13 pigment groups) of marine phytoplankton, and the relevance for pulse-amplitude-modulated and fast-repetition-rate fluorometry. *J Phycol*, **43**, 1236-1251. https://doi.org/10.1111/j.1529-8817.2007.00422.x

Juhas, M., von Zadow, A., Spexard, M., Schmidt, M., Kottke, T. and Buchel, C. (2014) A novel cryptochrome in the diatom *Phaeodactylum tricornutum* influences the regulation of light-harvesting protein levels. *Febs J*, **281**, 2299-2311. https://doi.org/10.1111/Febs.12782

Junglas, B. and Schneider, D. (2018) What is Vipp1 good for? *Mol Microbiol*, **108**, 1-5. https://doi.org/10.1111/mmi.13924

Järvi, S., Suorsa, M. and Aro, E.M. (2015) Photosystem II repair in plant chloroplasts - Regulation, assisting proteins and shared components with photosystem II biogenesis. *Bba-Bioenergetics*, **1847**, 900-909. https://doi.org/10.1016/j.bbabio.2015.01.006

Kil, Y.J., Becker, C., Sandoval, W., Goldberg, D. and Bern, M. (2011) Preview: a program for surveying shotgun proteomics tandem mass spectrometry data. *Anal Chem*, **83**, 5259-5267. https://doi.org/10.1021/ac200609a

Kirst, H., Formighieri, C. and Melis, A. (2014) Maximizing photosynthetic efficiency and culture productivity in cyanobacteria upon minimizing the phycobilisome light-harvesting antenna size. *Bba-Bioenergetics*, **1837**, 1653-1664. https://doi.org/10.1016/j.bbabio.2014.07.009

Kirst, H., Garcia-Cerdan, J.G., Zurbriggen, A. and Melis, A. (2012a) Assembly of the light-harvesting chlorophyll antenna in the green alga *Chlamydomonas reinhardtii* requires expression of the TLA2-CpFTSY gene. *Plant Physiol*, **158**, 930-945. https://doi.org/10.1104/pp.111.189910

Kirst, H., Garcia-Cerdan, J.G., Zurbriggen, A., Ruehle, T. and Melis, A. (2012b) Truncated photosystem chlorophyll antenna size in the green microalga *Chlamydomonas reinhardtii* upon deletion of the TLA3-CpSRP43 gene. *Plant Physiol*, **160**, 2251-2260. https://doi.org/10.1104/pp.112.206672

Kirst, H. and Melis, A. (2014) The chloroplast signal recognition particle (CpSRP) pathway as a tool to minimize chlorophyll antenna size and maximize photosynthetic productivity. *Biotechnol Adv*, **32**, 66-72. https://doi.org/10.1016/j.biotechadv.2013.08.018

Lang, M. and Kroth, P.G. (2001) Diatom fucoxanthin chlorophyll a/c-binding protein (FCP) and land plant light-harvesting proteins use a similar pathway for thylakoid membrane Insertion. *J Biol Chem*, **276**, 7985-7991. https://doi.org/10.1074/jbc.M006417200

Lavaud, J. and Goss, R. (2014) The peculiar features of non-photochemical fluorescence quenching in diatoms and brown algae. In *Non-photochemical quenching and energy dissipation in plants, algae and cyanobacteria. Advances in photosynthesis and respiration (Including*

bioenergy and related processes) (Demmig-Adams, B., Garab, G., Adams, I.W. and Govindjee eds). Dordrecht: Springer, pp. 421-443.

Levitan, O., Chen, M., Kuang, X., Cheong, K.Y., Jiang, J., Banal, M., Nambiar, N., Gorbunov, M.Y., Ludtke, S.J., Falkowski, P.G. and Dai, W. (2019) Structural and functional analyses of photosystem II in the marine diatom *Phaeodactylum tricornutum*. *Proc Natl Acad Sci U S A*, **116**, 17316-17322. https://doi.org/10.1073/pnas.1906726116

Liu, C.M., Willmund, F., Golecki, J.R., Cacace, S., Hess, B., Markert, C. and Schroda, M. (2007) The chloroplast HSP70B-CDJ2-CGE1 chaperones catalyse assembly and disassembly of VIPP1 oligomers in *Chlamydomonas*. *Plant J*, **50**, 265-277. https://doi.org/10.1111/j.1365-313X.2007.03047.x

Mishra, M., Arukha, A.P., Bashir, T., Yadav, D. and Prasad, G.B.K.S. (2017) All new faces of diatoms: Potential source of nanomaterials and beyond. *Front Microbiol*, **8**. https://doi.org/10.3389/fmicb.2017.01239

Mishra, R.C. and Grover, A. (2016) ClpB/Hsp100 proteins and heat stress tolerance in plants. *Crit Rev Biotechnol*, **36**, 862-874. https://doi.org/10.3109/07388551.2015.1051942

Mogk, A., Kummer, E. and Bukau, B. (2015) Cooperation of Hsp70 and Hsp100 chaperone machines in protein disaggregation. *Front Mol Biosci*, **2**, 22. https://doi.org/10.3389/fmolb.2015.00022

Mutka, S.C. and Walter, P. (2001) Multifaceted physiological response allows yeast to adapt to the loss of the signal recognition particle-dependent protein-targeting pathway. *Mol Biol Cell*, **12**, 577-588. https://doi.org/10.1091/mbc.12.3.577

Nelson, D.M., Treguer, P., Brzezinski, M.A., Leynaert, A. and Queguiner, B. (1995) Production and dissolution of biogenic silica in the ocean - Revised global estimates, comparison with regional data and relationship to biogenic sedimentation. *Global Biogeochem Cy*, **9**, 359-372. https://doi.org/10.1029/95gb01070

Nelson, N. and Ben-Shem, A. (2004) The complex architecture of oxygenic photosynthesis. *Nat Rev Mol Cell Biol*, **5**, 971-982. https://doi.org/10.1038/nrm1525

Nilsson, R., Brunner, J., Hoffman, N.E. and van Wijk, K.J. (1999) Interactions of ribosome nascent chain complexes of the chloroplast-encoded D1 thylakoid membrane protein with cpSRP54. *Embo J*, **18**, 733-742. https://doi.org/10.1093/emboj/18.3.733

Nilsson, R. and van Wijk, K.J. (2002) Transient interaction of cpSRP54 with elongating nascent chains of the chloroplast-encoded D1 protein; 'cpSRP54 caught in the act'. *FEBS Lett*, **524**, 127-133. https://doi.org/10.1016/s0014-5793(02)03016-8

Nordhues, A., Schottler, M.A., Unger, A.K., Geimer, S., Schonfelder, S., Schmollinger, S., Rutgers, M., Finazzi, G., Soppa, B., Sommer, F., Muhlhaus, T., Roach, T., Krieger-Liszkay, A., Lokstein, H., Crespo, J.L. and Schroda, M. (2012) Evidence for a role of VIPP1 in the structural organization of the photosynthetic apparatus in *Chlamydomonas*. *Plant Cell*, **24**, 637-659. https://doi.org/10.1105/tpc.111.092692

Nymark, M., Sharma, A.K., Hafskjold, M.C., Sparstad, T., Bones, A.M. and Winge, P. (2017) CRISPR/Cas9 Gene editing in the marine diatom *Phaeodactylum tricornutum*. *Bio-protocol* **7**, e2442. https://doi.org/10.21769/BioProtoc.2442

Nymark, M., Sharma, A.K., Sparstad, T., Bones, A.M. and Winge, P. (2016) A CRISPR/Cas9 system adapted for gene editing in marine algae. *Sci Rep-Uk*, **6**. https://doi.org/10.1038/srep24951

Nymark, M., Valle, K.C., Brembu, T., Hancke, K., Winge, P., Andresen, K., Johnsen, G. and Bones, A.M. (2009) An integrated analysis of molecular acclimation to high light in the marine diatom *Phaeodactylum tricornutum*. *PLoS ONE*, **4**, e7743.

https://doi.org/10.1371/journal.pone.0007743
Nymark, M., Valle, K.C., Hancke, K., Winge, P., Andresen, K., Johnsen, G., Bones, A.M. and Brembu, T. (2013) Molecular and photosynthetic responses to prolonged darkness and subsequent acclimation to re-illumination in the diatom *Phaeodactylum tricornutum*. *PLoS ONE*, **8**, e58722. https://doi.org/10.1371/journal.pone.0058722
Nymark, M., Volpe, C., Hafskjold, M.C.G., Kirst, H., Serif, M., Vadstein, O., Bones, A.M., Melis, A. and Winge, P. (2019) Loss of ALBINO3b insertase results in truncated light-harvesting antenna in diatoms. *Plant Physiol*, **181**, 1257-1276. https://doi.org/10.1104/pp.19.00868
Ouyang, M., Li, X., Ma, J., Chi, W., Xiao, J., Zou, M., Chen, F., Lu, C. and Zhang, L. (2011) LTD is a protein required for sorting light-harvesting chlorophyll-binding proteins to the chloroplast SRP pathway. *Nat Commun*, **2**, 277. https://doi.org/10.1038/ncomms1278
Perez-Riverol, Y., Csordas, A., Bai, J.W., Bernal-Llinares, M., Hewapathirana, S., Kundu, D.J., Inuganti, A., Griss, J., Mayer, G., Eisenacher, M., Perez, E., Uszkoreit, J., Pfeuffer, J., Sachsenberg, T., Yilmaz, S., Tiwary, S., Cox, J., Audain, E., Walzer, M., Jarnuczak, A.F., Ternent, T., Brazma, A. and Vizcaino, J.A. (2019) The PRIDE database and related tools and resources in 2019: improving support for quantification data. *Nucleic Acids Res*, **47**, D442-D450. https://doi.org/10.1093/nar/gky1106
Pilgrim, M.L., van Wijk, K.J., Parry, D.H., Sy, D.A. and Hoffman, N.E. (1998) Expression of a dominant negative form of cpSRP54 inhibits chloroplast biogenesis in *Arabidopsis*. *Plant J*, **13**, 177-186. https://doi.org/10.1046/j.1365-313x.1998.00021.x
Piskozub, M., Kroliczewska, B. and Kroliczewski, J. (2015) Ribosome nascent chain complexes of the chloroplast-encoded cytochrome b6 thylakoid membrane protein interact with cpSRP54 but not with cpSecY. *J Bioenerg Biomembr*, **47**, 265-278. https://doi.org/10.1007/s10863-014-9598-0
Pool, M.R. (2005) Signal recognition particles in chloroplasts, bacteria, yeast and mammals (review). *Mol Membr Biol*, **22**, 3-15. https://doi.org/10.1080/09687860400026348
Ridley, S.M. and Ridley, J. (1979) Interaction of chloroplasts with inhibitors: Location of carotenoid synthesis and inhibition during chloroplast development. *Plant Physiol*, **63**, 392-398. https://doi.org/10.1104/pp.63.2.392
Ries, F., Herkt, C. and Willmund, F. (2020) Co-translational protein folding and sorting in chloroplasts. *Plants-Basel*, **9**. https://doi.org/10.3390/plants9020214
Rodriguez, F., Chauton, M., Johnsen, G., Andresen, K., Olsen, L.M. and Zapata, M. (2006) Photoacclimation in phytoplankton: implications for biomass estimates, pigment functionality and chemotaxonomy. *Mar Biol*, **148**, 963-971. https://doi.org/10.1007/s00227-005-0138-7
Rokka, A., Suorsa, M., Saleem, A., Battchikova, N. and Aro, E.M. (2005) Synthesis and assembly of thylakoid protein complexes: multiple assembly steps of photosystem II. *Biochem J*, **388**, 159-168. https://doi.org/10.1042/Bj20042098
Rutschow, H., Ytterberg, A.J., Friso, G., Nilsson, R. and van Wijk, K.J. (2008) Quantitative proteomics of a chloroplast SRP54 sorting mutant and its genetic interactions with CLPC1 in Arabidopsis. *Plant Physiol*, **148**, 156-175. https://doi.org/10.1104/pp.108.124545
Rütgers, M. and Schroda, M. (2013) A role of VIPP1 as a dynamic structure within thylakoid centers as sites of photosystem biogenesis. *Plant Signal. Behav.*, **8**, e27037. https://doi.org/10.4161/psb.27037
Serôdio, J., Vieira, S., Cruz, S. and Coelho, H. (2006) Rapid light-response curves of chlorophyll fluorescence in microalgae: relationship to steady-state light curves and non-photochemical quenching in benthic diatom-dominated assemblages. *Photosynth Res*, **90**, 29-43.

https://doi.org/10.1007/s11120-006-9105-5
Siebenaller, C., Junglas, B. and Schneider, D. (2019) Functional implications of multiple IM30 oligomeric states. *Front Plant Sci*, **10**. https://doi.org/10.3389/fpls.2019.01500
Sundberg, E., Slagter, J.G., Fridborg, I., Cleary, S.P., Robinson, C. and Coupland, G. (1997) ALBINO3, an Arabidopsis nuclear gene essential for chloroplast differentiation, encodes a chloroplast protein that shows homology to proteins present in bacterial membranes and yeast mitochondria. *Plant Cell*, **9**, 717-730. https://doi.org/10.1105/tpc.9.5.717
Suomi, T., Seyednasrollah, F., Jaakkola, M.K., Faux, T. and Elo, L.L. (2017) ROTS: An R package for reproducibility-optimized statistical testing. *PLoS Comput Biol*, **13**. https://doi.org/10.1371/journal.pcbi.1005562
Theis, J., Niemeyer, J., Schmollinger, S., Ries, F., Rutgers, M., Gupta, T.K., Sommer, F., Muranaka, L.S., Venn, B., Schulz-Raffelt, M., Willmund, F., Engel, B.D. and Schroda, M. (2020) VIPP2 interacts with VIPP1 and HSP22E/F at chloroplast membranes and modulates a retrograde signal for *HSP22E/F* gene expression. *Plant Cell Environ*, **43**, 1212-1229. https://doi.org/10.1111/pce.13732
Theis, J. and Schroda, M. (2016) Revisiting the photosystem II repair cycle. *Plant Signal Behav*, **11**, e1218587. https://doi.org/10.1080/15592324.2016.1218587
Träger, C., Rosenblad, M.A., Ziehe, D., Garcia-Petit, C., Schrader, L., Kock, K., Richter, C.V., Klinkert, B., Narberhaus, F., Herrmann, C., Hofmann, E., Aronsson, H. and Schunemann, D. (2012) Evolution from the prokaryotic to the higher plant chloroplast signal recognition particle: the signal recognition particle RNA is conserved in plastids of a wide range of photosynthetic organisms. *Plant Cell*, **24**, 4819-4836. https://doi.org/10.1105/tpc.112.102996
Trösch, R., Mühlhaus, T., Schroda, M. and Willmund, F. (2015) ATP-dependent molecular chaperones in plastids - More complex than expected. *Bba-Bioenergetics*, **1847**, 872-888. https://doi.org/10.1016/j.bbabio.2015.01.002
Walter, B., Hristou, A., Nowaczyk, M.M. and Schünemann, D. (2015a) *In vitro* reconstitution of co-translational D1 insertion reveals a role of the cpSec-Alb3 translocase and Vipp1 in photosystem II biogenesis. *Biochem J*, **468**, 315-324. https://doi.org/10.1042/Bj20141425
Walter, B., Pieta, T. and Schunemann, D. (2015b) *Arabidopsis thaliana* mutants lacking cpFtsY or cpSRP54 exhibit different defects in photosystem II repair. *Front Plant Sci*, **6**, 250. https://doi.org/10.3389/fpls.2015.00250
Waterhouse, A., Bertoni, M., Bienert, S., Studer, G., Tauriello, G., Gumienny, R., Heer, F.T., de Beer, T.A.P., Rempfer, C., Bordoli, L., Lepore, R. and Schwede, T. (2018) SWISS-MODEL: homology modelling of protein structures and complexes. *Nucleic Acids Res*, **46**, W296-W303. https://doi.org/10.1093/nar/gky427
Wickström, D., Wagner, S., Baars, L., Ytterberg, A.J., Klepsch, M., van Wijk, K.J., Luirink, J. and de Gier, J.W. (2011) Consequences of depletion of the signal recognition particle in *Escherichia coli*. *J Biol Chem*, **286**, 4598-4609. https://doi.org/10.1074/jbc.M109.081935
Witt, H.T. (1979) Energy conversion in the functional membrane of photosynthesis. Analysis by light pulse and electric pulse methods. The central role of the electric field. *Biochim Biophys Acta*, **505**, 355-427. https://doi.org/10.1016/0304-4173(79)90008-9
Wu, H.Y., Cockshutt, A.M., McCarthy, A. and Campbell, D.A. (2011) Distinctive photosystem II photoinactivation and protein dynamics in marine diatoms. *Plant Physiol*, **156**, 2184-2195. https://doi.org/10.1104/pp.111.178772
Wu, H.Y., Roy, S., Alami, M., Green, B.R. and Campbell, D.A. (2012) Photosystem II photoinactivation, repair, and protection in marine centric diatoms. *Plant Physiol*, **160**, 464-

476. https://doi.org/10.1104/pp.112.203067
Zhang, D., Sweredoski, M.J., Graham, R.L., Hess, S. and Shan, S.O. (2012) Novel proteomic tools reveal essential roles of SRP and importance of proper membrane protein biogenesis. *Mol Cell Proteomics*, **11**, M111 011585. https://doi.org/10.1074/mcp.M111.011585
Ziehe, D., Dunschede, B. and Schunemann, D. (2017) From bacteria to chloroplasts: evolution of the chloroplast SRP system. *Biol Chem*, **398**, 653-661. https://doi.org/10.1515/hsz-2016-0292
Ziehe, D., Dunschede, B. and Schunemann, D. (2018) Molecular mechanism of SRP-dependent light-harvesting protein transport to the thylakoid membrane in plants. *Photosynth Res*, **138**, 303-313. https://doi.org/10.1007/s11120-018-0544-6

Table 1. Growth rates of WT and *cpsrp54* mutant lines acclimated to different light intensities. Maximum cell divisions per day during the exponential phase were calculated from three biological replicates of WT and *cpsrp54* KO lines acclimated to LL (35 µmol photons m^{-2} s^{-1}), ML (200 µmol photons m^{-2} s^{-1}) and HL (1000 µmol photons m^{-2} s^{-1}). Values are presented with ±SD.

Table 2. Proteomics data. Proteins encoded in the chloroplast genome or predicted to contain chloroplast transit peptides sequences that were significantly regulated (FDR <0.01) in the same direction in both *cpsrp54-8 and cpsrp54-11* lines compared to WT after 6 h in ML showing $\log_2$ ratios ≥ ± 0.5 for at least one of the mutant lines and where at least two unique peptides were detected. Only proteins with a Score sequest HT >10 were included in the table. Ratios were calculated based on results from five biological replicates for each line. Downregulated proteins are marked in bold. †Low molecular weight proteins included despite detection of only one unique peptide. The abbreviations used are: Psa: PSI proteins; Psb: PSII proteins; FNR: ferredoxin NAPD(H) reductase; atp: chloroplast ATP synthase proteins; LHCX: light-harvesting complex stress-related proteins; APX: Ascorbate peroxidase; VIPP1: vesicle-inducing protein in plastids 1; ClpB: Caseinolytic proteases of subfamily B; chlI: Magnesium chelatase I subunit; HEMB: porphobilinogen synthase; rps13: 30S ribosomal protein S13; sCdc48: SELMA Cell division cycle 48; IPMDH: isopropylmalate dehydrogenase; FbaC2: Fructose-1,6-bisphosphate aldolase C2

Table 3. Overview of the effect of loss of CpSRP54 in diatom (*P. tricornutum*), plant (*A. thaliana*) and green algae (*C. reinhardtii*) model organisms. Symbols and abbreviations used are NC = no change; ↓ = downregulated compared to WT; ↑ = upregulated compared to WT; n/a = not assessed

Figure 1. Structural features of diatom CpSRP54 proteins. a) Schematic view of the conserved domains of CpSRP54. The area of the CpSRP54 protein corresponding to the 20-bp target region for CRISPR/Cas9-based gene editing is located in the N-terminal helical bundle domain (N-domain),

with the protospacer adjacent motif (PAM) target site located at the forward DNA strand (green character). The diatom and *Bolidophytes* native insertion sequence between the G1 and G2 domains are shown above the figure. CTP: chloroplast-targeting peptide; V: variable domain; N: SRP54 N-terminal helical bundle domain; G: SRP GTPase containing domain; M: SRP54 signal peptide binding domain. **b)** Protein alignment showing the insert region between the G1 and G2 domains in diatoms. **c)** Protein model of diatom CpSRP54 highlighting the insert region (dots) and the docking site with FTSY. **d)** Protein alignment of the C-terminal region of the M-domain containing the conserved RR-motif. **e)** Overview of amino acid sequences resulting from CRISPR/Cas9-mediated indels in the three *cpsrp54* knock out lines, causing premature stop codons and truncated CpSRP54 proteins. The A1 allele in *cpsrp54-20* could not be amplified by PCR and is indicated by "?". Color coding is as follows: Wild-type (WT) target sequence: blue characters; altered amino acids as a result of indels: red characters. Asterisks indicate premature stops.

Figure 2. Color and spectral properties of WT and *cpsrp54* mutants. a) Culture color of LL-acclimated WT and *cpsrp54* mutants at equal cell densities. **b)** *In vivo* fluorescence excitation spectra and **c)** absorbance spectra of cultures acclimated to LL. Fluorescence emission was measured at 730 nm to allow for full visible range (400 – 700 nm) fluorescence excitation. Presented spectra for all lines are representative of three replicates per line.

Figure 3. Pigment levels, DES index and NPQ capacity in WT and *cpsrp54* mutant cell lines. Cellular pigment contents (fmol/cell) are shown for **a)** Chl *a*, **b)** Fx, **c)** Ddx, and **d)** Dtx in WT and *cpsrp54* mutant cells as a function of time following a shift from LL conditions (0 h; 35 µmol photons m^{-2} s^{-1}) to ML conditions (200 µmol photons m^{-2} s^{-1}) for 0.5, 6, 24, 48, and 168 h. **e)** DES index [DES = Dtx/(Dtx + Ddx)] calculated from data shown in C and D. **f)** Induction of NPQ as a function of increasing light intensity was calculated from rapid light curves derived from LL-acclimated cells. NPQ = ($F_{m'max}/F_{m'}$) - 1. $F_{m'max}$ replaces the commonly used F_m, since $F_{m'}$ values frequently occur at low light intensities that are higher than the F_m from dark-treated diatom samples (Serôdio *et al.*, 2006). Results are presented as means of three biological replicates ±SD. Black circles indicate individual data points for the replicates. Asterisks describe significant differences between *cpsrp54* mutants and WT as indicated by two-way ANOVA with Dunnet's multiple comparison tests ($p < 0.05$).

Figure 4. Photophysiological responses of WT and *cpsrp54* mutant cell lines after a shift from LL to ML conditions. a) Photosynthetic (PSII) efficiency (F_v/F_m), **b)** Maximum light-utilization coefficient (α), **c)** Photosynthetic capacity ($rETR_{max}$), and **d)** Light saturation index (E_k) in WT and *cpsrp54* mutant cells as a function of time following a shift from LL conditions (0 h; 35 µmol photons m^{-2} s^{-1}) to ML conditions (200 µmol photons m^{-2} s^{-1}) for 0.5, 6, 24, 48, and 168 h. **e)** In vivo assessment of PSII/PSI reaction centers ratios and **f)** Photosynthetic electron flow in LL and ML-acclimated cultures. Results are presented as means of three biological replicates ±SD. Black circles indicate individual data points for the replicates. Asterisks indicate the results of two-way ANOVA with Dunnet's multiple comparison test ($p < 0.05$)

Figure 5. Photosynthetic efficiency (F_v/F_m) in WT and *cpsrp54* mutant lines as a response to HL with or without addition of the chloroplast protein synthesis inhibitor lincomycin (LINC). LL-acclimated WT and *cpsrp54* lines was treated with or without lincomycin (LINC) before exposure to 60 min of HL (1000 µmol photons m^{-2} s^{-1}) followed by 30 min recovery in dim light. WT data are presented as averages of three biological replicates ± SD. *Cpsrp54* data are averages of the three *cpsrp54* lines 8, 11 and 20, three biological replicates of each line (in total n = 9) ± SD.

Figure 6. Analysis of thylakoid membrane protein accumulation at different light conditions in WT and *cpsrp54* mutant lines. a) Abundance of FCP proteins belonging to the LHCF group and PSII core proteins D1 and D2 in LL-acclimated cells, after 6h in ML and in cells acclimated to ML. The LHCF antibody is predicted to detect LHCF1-11 (Juhas *et al.*, 2014). An antibody recognizing the β-subunit of ATP synthase (AtpB) was used as loading control on each of the individual blots. Images have been cropped. Relative quantification of **b)** LHCF1-11, **c)** D1 and **d)** D2 protein accumulation in *cpsrp54* lines compared to WT in LL and ML-acclimated cells was performed using ImageJ to estimate band intensity. All values were normalized against AtpB included as a loading control on all blots. Ratios presented are an average of results calculated from two independent experiments and minimum three different blots with 1-3 biological replicates included in each blot. 10 µg total protein was loaded in each well. Black circles indicate individual data points for the replicates.

Figure 7. Models of the CpSRP pathway for integration of thylakoid membrane (TM) proteins in *P. tricornutum* compared to plant (*A. thaliana*) and green algae (*C. reinhardtii*) model organisms. a) Schematic overview of the suggested roles of members of the CpSRP pathway in *P. tricornutum*. CpSRP54, likely in interaction with its receptor CpFTSY, are proposed to guide translating ribosomes to the ALB3a insertase and possibly the CpSecY translocase for co-translational insertion of chloroplast encoded TM proteins (right side). FCP proteins synthesized by ribosomes on the chloroplast endoplasmic reticulum membrane (cERM) are transported through the four membranes surrounding diatom chloroplasts and eventually delivered to ALB3b in an unknown manner independent of the CpSRP pathway (left side). **b)** Schematic overview of the roles of members of the CpSRP pathway in *A. thaliana*. Several members of the CpSRP pathway (CpSRP54, CpFTSY; ALB3) have dual roles and function in both post-translational insertion of LHCPs (left side) and co-translational insertion of chloroplast encoded proteins (right side) into the TM membrane. LTD and CpSRP43 of the post-translational CpSRP pathway are not present in diatom genomes. LTD delivers LHCPs to the CpSRP43/CpSRP54 complex that in the next step interacts with CpFTSY before integration of LHCPs into TMs through ALB3. **c)** Schematic overview of the roles of members of the CpSRP pathway in *C. reinhardtii*. The CpSRP pathway of *C. reinhardtii* comprises mostly the same key molecular players as *A. thaliana*, but CpSRP54 and CpFTSY are proposed to function exclusively in the post-translational CpSRP pathway. Here CpSRP54 is not complexed to CpSRP43, but CpSRP54 is believed to function further downstream. Similar to diatoms, but in contrast to plants, two different ALB3 insertases function in the post- and co-translational CpSRP pathway.
Abbreviations used are: cERM: chloroplast endoplasmic reticulum membrane; PPM: periplastidial membrane; OEM: outer envelope membrane; IEM: inner envelope membrane; FCP: Fx-Chl *a/c*-binding proteins; LHCP: Light harvesting complex proteins; LTD: LHCP translocation defect protein; Cp: Chloroplast; SRP: signal recognition particle.

Table 1.

	35 µmol $s^{-1}m^{-2}$	200 µmol $s^{-1}m^{-2}$	1000 µmol $s^{-1}m^{-2}$
WT	1.54 ± 0.24	2.23 ± 0.03	2.03 ± 0.18
cpsrp54-8	1.41 ± 0.18	1.61 ± 0.14	1.55 ± 0.03
cpsrp54-11	1.38 ± 0.26	1.75 ± 0.09	1.46 ± 0.15
cpsrp54-20	1.38 ± 0.28	1.77 ± 0.12	1.60 ± 0.06

1263 **Table 2.**

Protein ID	Name	Function (predicted)	Location (predicted)	Nucleus (N)/Chloroplast (C)-encoded	*cpsrp54-8*/WT (log_2 ratio)	*cpsrp54-11*/WT (log_2 ratio)	# unique peptides	# peptides	Score sequest HT
A0T096	CP43 (PsbC)	PSII core	TM	C	**-0.58**	**-0.44**	9	9	51.1
A0T097	D2 (PsbD)	PSII core	TM	C	**-2.03**	**-0.69**	2	2	10.85
A0T0G0	PsbY†	PSII core	TM	C	**-0.93**	**-1.31**	1	1	14.09
B7G6V4	PsbP	PSII OEC	TM	N	0.39	0.65	4	4	11.02
A0T0C9	PetA	$Cytb_6f$	TM	C	**-0.78**	**-0.47**	10	10	63.72
B5Y3C9	PetC2	$Cytb_6f$	TM	N	**-0.56**	**-0.49**	5	5	11.94
A0T0L2	PsaC	PSI core	TM	C	**-0.34**	**-0.65**	4	4	24.56
A0T0B9	PsaD	PSI core	TM	C	**-0.41**	**-0.73**	7	7	24.3
A0T0F3	PsaE†	PSI core	TM	C	**-0.71**	**-0.61**	1	1	26.67
A0T0M1	PsaF	PSI core	TM	C	**-0.53**	**-0.56**	3	3	49.68
A0T0M6	PsaL	PSI core	TM	C	**-0.51**	**-0.62**	2	2	18.61
B7GCT8	FNR	Ferredoxin-NADP reductase	Stroma/TM bound	N	0.80	0.66	8	10	248.79
B7G0M5	FNR	Ferredoxin-NADP reductase	Stroma/TM bound	N	1.34	1.44	4	6	53.69
A0T0F1	atpA	ATP synthase	TM	C	**-0.33**	**-0.63**	16	19	178.79
A0T0F0	atpD	ATP synthase	TM	C	**-1.12**	**-0.62**	4	4	12.1
B7FYL0	LHCX1	Photoprotection	TM	N	0.35	0.79	4	4	46.83
B7FR60	LHCX2	Photoprotection	TM	N	0.56	0.59	3	3	108.13
B7G386	APX	ROS scavenging	TM-bound	N	0.61	0.64	13	13	101.35
B7FU48	Cyclophilin type peptidyl-prolyl cis-trans isomerase	Formation of PSII	Lumen	N	0.68	0.54	4	4	22.24
B7FWP5	VIPP1	TM biogenesis/ /remodeling, PSII biogenesis	TM surface, stroma	N	0.90	0.76	7	7	30.86
B5Y3P1	DNAJ	Co-chaperone	Stroma	N	0.48	0.55	7	7	27.24
A0T0H7	DnaK	Chaperone	Stroma	C	1.48	1.62	35	35	244.61
B5Y5I5	ClpB	Chaperone	Stroma	N	0.68	0.61	9	9	40.91
B7FVE3	Tic62-NAD(P)-related group II protein	Unknown	Chloroplast	N	0.30	0.71	3	3	10.07
B7FUD8	Tic62-NAD(P)-related group II protein	Unknown	Chloroplast	N	1.06	0.69	4	4	22.86
B7FPG9	Oligopeptidase A	Hydrolysis of peptide bond	Chloroplast	N	0.70	0.55	8	8	51.31
A0T0B5	chlI	Biosynthesis of Chl	Stroma	C	**-0.57**	**-0.57**	6	6	12

B7FSN7	AlaD (HemB)	Biosynthesis of Chl	Stroma	N	0.69	0.70	5	5		24.11
A0T0J8	rps13	Translation	Chloroplast	C	**-0.65**	**-0.52**	3	3		29.5
B7G1T3	sCdc48	Degradation of chloroplast membrane proteins	Chloroplast membrane-associated	N	**-0.53**	**-0.51**	5	6		11.81
B5Y3B2	Myo-inositol 2-dehydrogenase	Metabolism	Chloroplast	N	1.22	0.88	2	2		17.17
B7G1X8	IPMDH	Amino-acid biosynthesis	Stroma	N	**-0.96**	**-0.80**	6	6		27.81
B7G9G9	FbaC2	Carbohydrate metabolism	Stroma	N	0.44	0.71	5	5		35.95

1277 **Table 3.**

Effects of loss of CpSRP54	***P. tricornutum***	***A. thaliana***	***C. reinhardtii***	***References***
Color	NC	↓	↓	Present paper; Amin *et al*., 1999; Rutschow *et al*., 2008; Jeong *et al*., 2017
LHC proteins	NC	↓	↓	Present paper; Amin *et al*., 1999; Rutschow *et al*., 2008; Jeong *et al*., 2017
Proteins of photosynthetic complexes	↓	↓	NC	Present paper; Amin *et al*., 1999; Rutschow *et al*., 2008; Hristou *et al*., 2029; Jeong *et al*., 2017
Light harvesting pigments	NC	↓	↓	Present paper; Amin *et al*., 1999; Jeong *et al*., 2017
Photoprotective pigments during light stress	↑	n/a	n/a	Present paper
Chaperones (compensating mechanisms)	↑	↑	n/a	Present paper; Amin *et al*., 1999; Rutschow *et al*., 2008
Growth in low light intensities	NC	↓	n/a	Present paper; Rutschow *et al*., 2008
Growth at higher light intensities	↓	↓	↑	Present paper; Rutschow *et al*., 2008; Jeong *et al*., 2017
Photosynthetic performance in low light	NC	NC	NC	Present paper; Hutin *et al*., 2002; Jeong *et al*., 2017
Photosynthetic performance at higher light intensities	↓	↓	NC	Present paper; Hutin *et al*., 2002; Jeong *et al*., 2017
PSII repair	↓	↓	n/a	Present paper; Walter ***et al***., 2015

1278

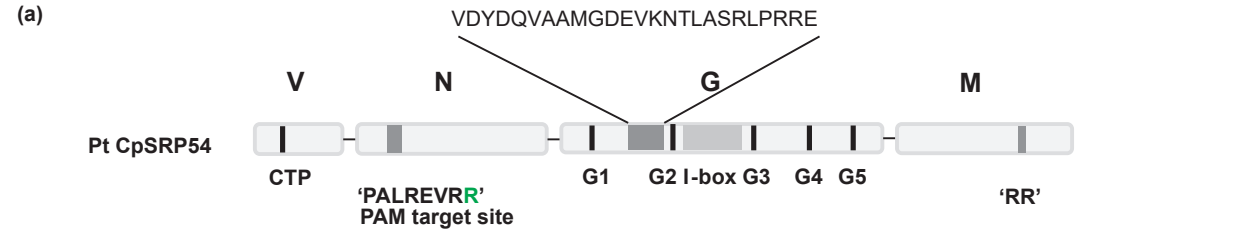
(a)
VDYDQVAAMGDEVKNTLASRLPRRE
V
N
G
M
Pt CpSRP54
CTP
'PALREVRR'
PAM target site
G1
G2 I-box G3
G4
G5
'RR'

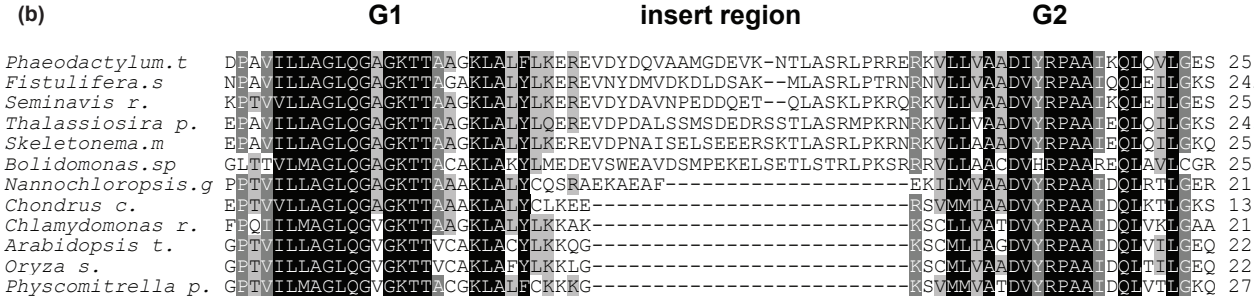
(b)
G1
insert region
G2
Phaeodactylum.t DPAVILLAGLQGAGKTTAAGKLALFLKEREVDYDQVAAMGDEVK-NTLASRLPRREKVLLVAADIYRPAAIKQLQVLGES 251
Fistulifera.s NPAVILLAGLQGAGKTTAGAKLALYLKEREVNYDMVDKDLDSAK--MLASRLPTRNRNVLLVAADVYRPAAIQQLEILGKS 242
Seminavis r. KPTVVLLAGLQGAGKTTAAGKLALYLKEREVDYDAVNPEDDQET--QLASKLPKRQRKVLLVAADVYRPAAIKQLEILGES 256
Thalassiosira p. EPAVILLAGLQGAGKTTAAGKLALYLQEREVDPDALSSMSDEDRSSTLASRMPKRNRKVLLVAADVYRPAAIEQLQILGKS 243
Skeletonema.m EPAVILLAGLQGAGKTTAAGKLALYLKEREVDPNAISELSEEERSKTLASRLPKRNRKVLLAAADVYRPAAIEQLQILGKQ 259
Bolidomonas.sp GLTTVLMAGLQGAGKTTACAKLAKYLMEDEVSWEAVDSMPEKELSETLSTRLPKSRRRVLLAACDVHRPAAREQLAVLCGR 255
Nannochloropsis.g PPTVILLAGLQGAGKTTAAAKLALYCQSRAEKAEAF----------EKILMVAADVYRPAAIDQLRTLGER 219
Chondrus c. EPTVVLLAGLQGAGKTTAAAKLALYCLKEE----------RSVMMIAADVYRPAAIDQLKTLGKS 139
Chlamydomonas r. FPQIILMAGLQGVGKTTAAGKLALYLKKAK----------KSCLLVATDVYRPAAIDQLVKLGAA 218
Arabidopsis t. GPTVILLAGLQGVGKTTVCAKLACYLKKQG----------KSCMLIAGDVYRPAAIDQLVILGEQ 229
Oryza s. GPTVILLAGLQGVGKTTVCAKLAFYLKKLG----------KSCMLVAADVYRPAAIDQLTILGEQ 223
Physcomitrella p. GPTVILMAGLQGVGKTTACGKLALFCKKKG----------KSVMMVATDVYRPAAIDQLVTLGKQ 278

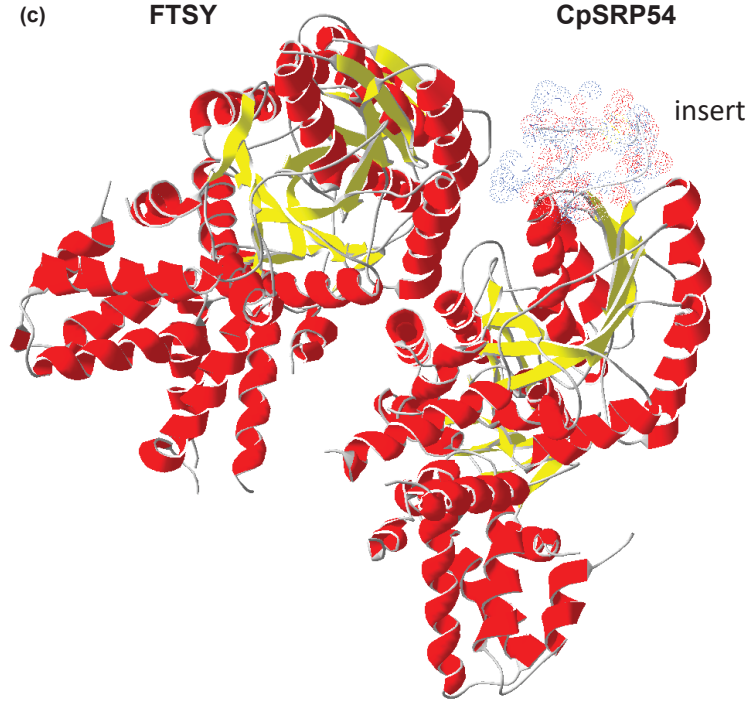
(c)
FTSY
CpSRP54
insert

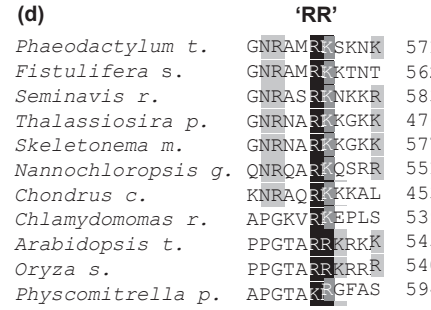
(d)
'RR'
Phaeodactylum t. GNRAMRKSKNK 571
Fistulifera s. GNRAMRKKTNT 562
Seminavis r. GNRASRKNKKR 583
Thalassiosira p. GNRNARKKGKK 476
Skeletonema m. GNRNARKKGKK 577
Nannochloropsis g. QNRQARKQSRR 551
Chondrus c. KNRAQRKKKAL 453
Chlamydomonas r. APGKVRKEPLS 539
Arabidopsis t. PPGTARRKRKK 545
Oryza s. PPGTARRKRRR 540
Physcomitrella p. APGTAKFGFAS 594

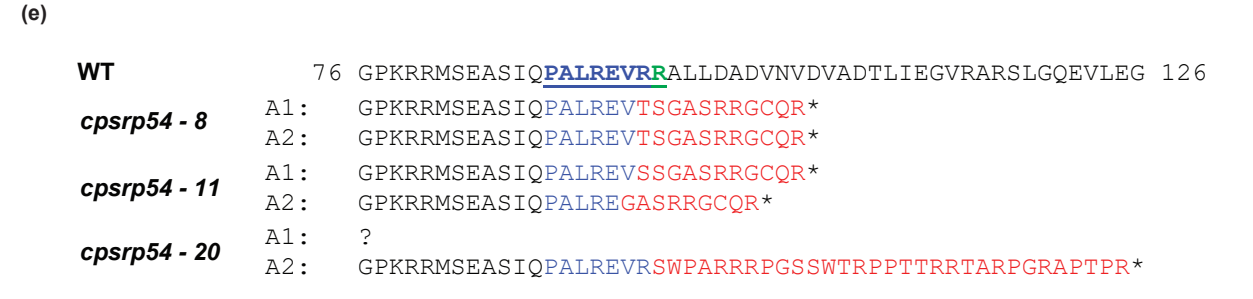
(e)
WT 76 GPKRRMSEASIQPALREVRRALLDADVNVDVADTLIEGVRARSLGQEVLEG 126
cpsrp54 - 8
A1: GPKRRMSEASIQPALREVTSGASRRGCQR*
A2: GPKRRMSEASIQPALREVTSGASRRGCQR*
cpsrp54 - 11
A1: GPKRRMSEASIQPALREVSSGASRRGCQR*
A2: GPKRRMSEASIQPALREGASRRGCQR*
cpsrp54 - 20
A1: ?
A2: GPKRRMSEASIQPALREVRSWPARRRPGSSWTRPPTTRRTARPGRAPTPR*

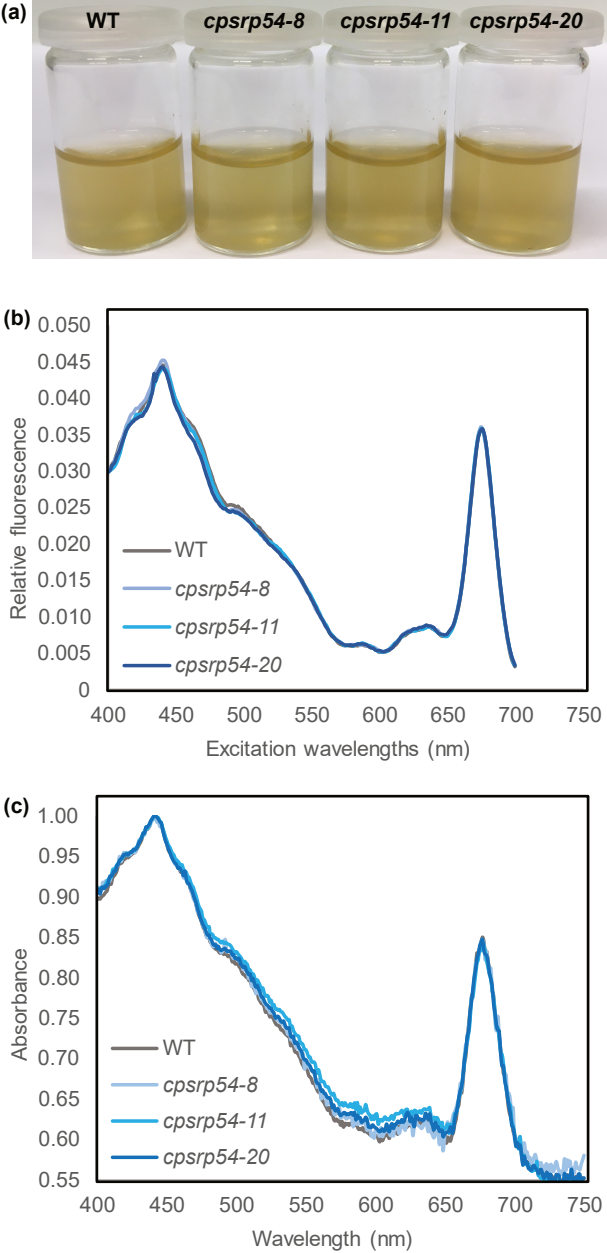
(a)
WT
cpsrp54-8
cpsrp54-11
cpsrp54-20
(b)
Relative fluorescence
0.050
0.045
0.040
0.035
0.030
0.025
0.020
0.015
0.010
0.005
0
WT
cpsrp54-8
cpsrp54-11
cpsrp54-20
400
450
500
550
600
650
700
750
Excitation wavelengths (nm)
(c)
Absorbance
1.00
0.95
0.90
0.85
0.80
0.75
0.70
0.65
0.60
0.55
WT
cpsrp54-8
cpsrp54-11
cpsrp54-20
400
450
500
550
600
650
700
750
Wavelength (nm)

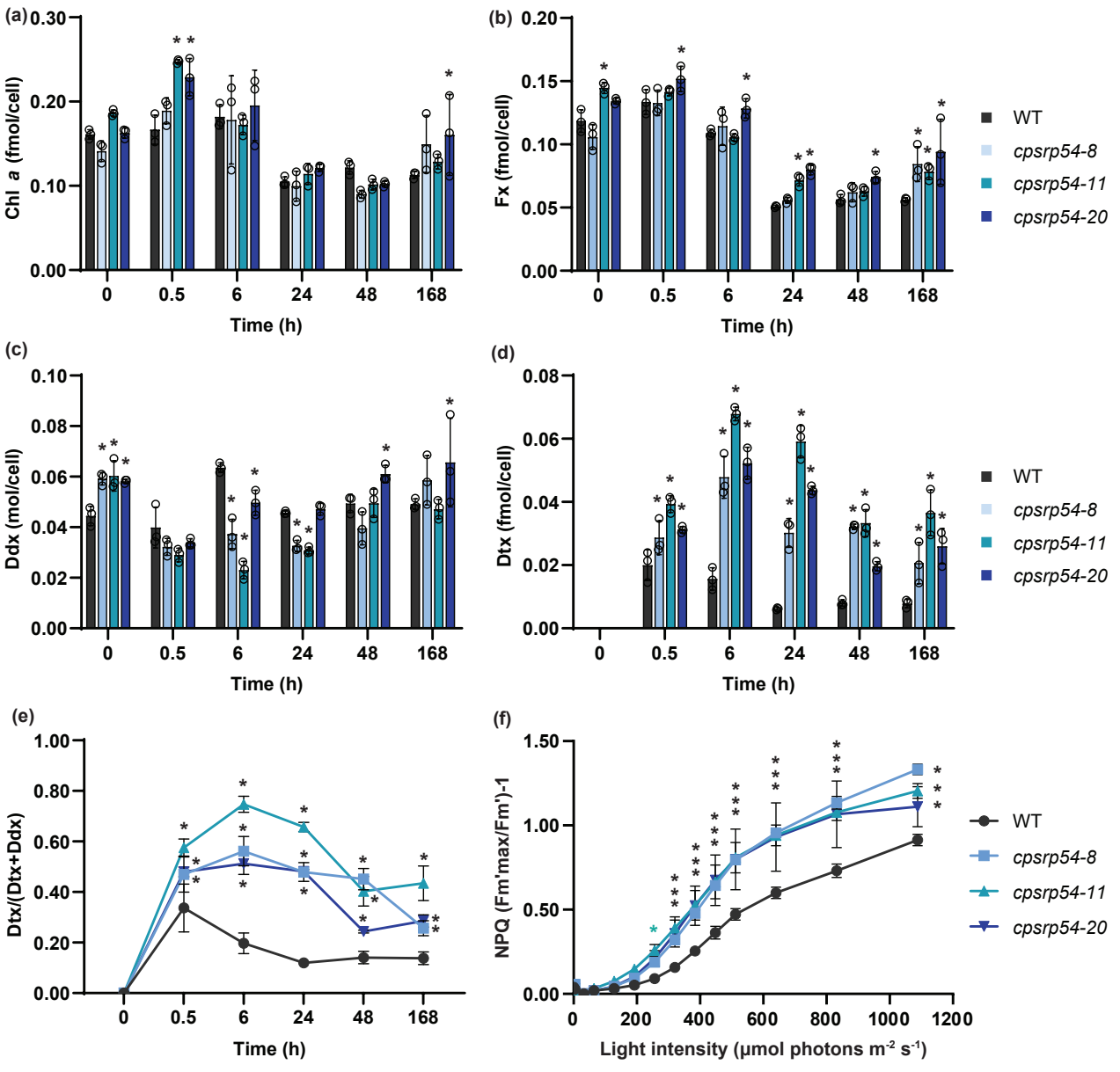
(a)
Chl a (fmol/cell)
0.30
0.20
0.10
0.00
0
0.5
6
24
48
168
Time (h)
(b)
Fx (fmol/cell)
0.20
0.15
0.10
0.05
0.00
Time (h)
WT
cpsrp54-8
cpsrp54-11
cpsrp54-20
(c)
Ddx (mol/cell)
0.10
0.08
0.06
0.04
0.02
0.00
Time (h)
(d)
Dtx (fmol/cell)
0.08
0.06
0.04
0.02
0.00
Time (h)
(e)
Dtx/(Dtx+Ddx)
1.00
0.80
0.60
0.40
0.20
0.00
Time (h)
(f)
NPQ (Fm'max/Fm')-1
1.50
1.00
0.50
0.00
0
200
400
600
800
1000
1200
Light intensity (µmol photons m-2 s-1)

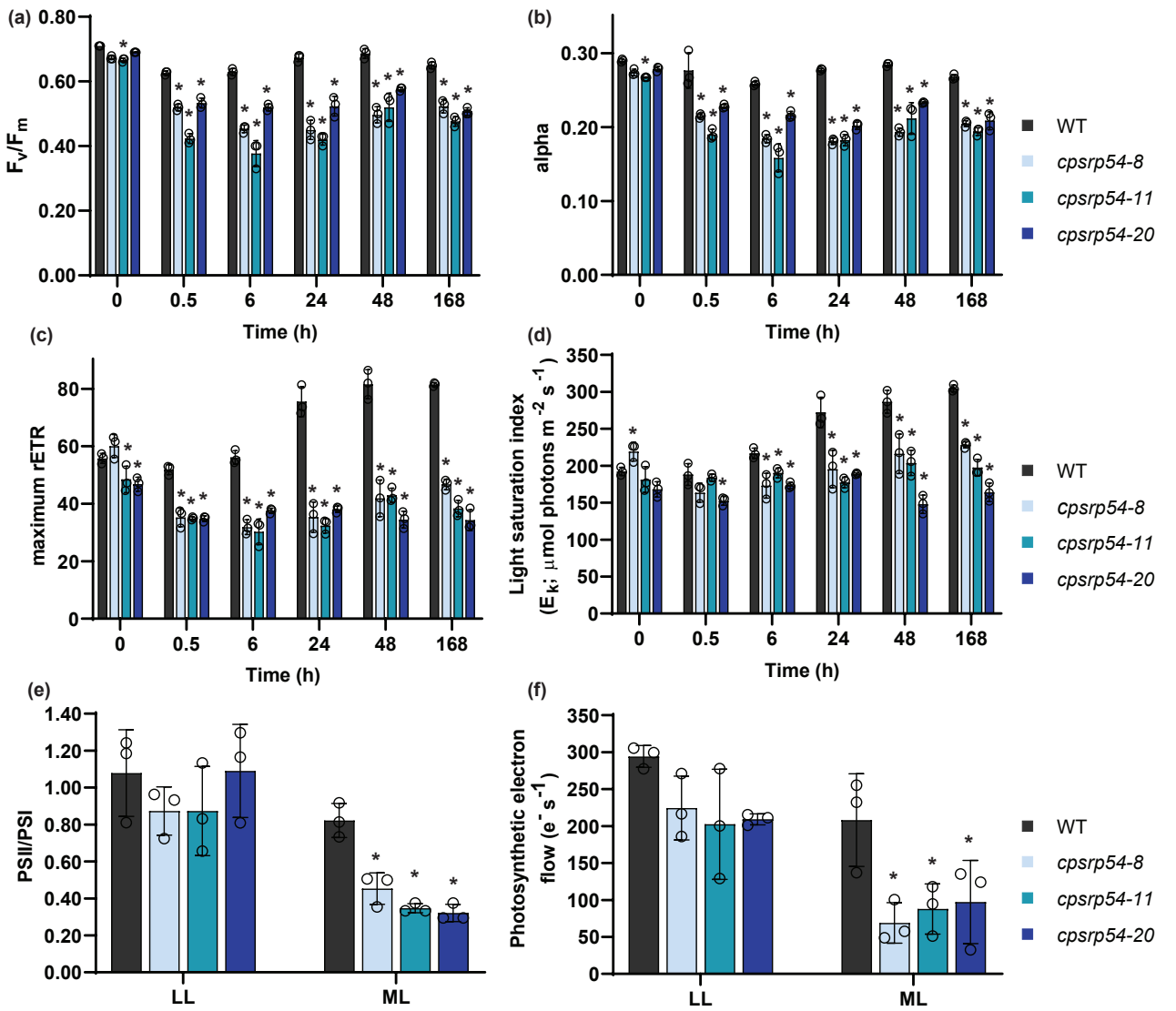
(a)
F_v/F_m
0.80
0.60
0.40
0.20
0.00
0
0.5
6
24
48
168
Time (h)
(b)
alpha
0.30
0.20
0.10
0.00
Time (h)
WT
cpsrp54-8
cpsrp54-11
cpsrp54-20
(c)
maximum rETR
80
60
40
20
0
Time (h)
(d)
Light saturation index
(E_k; μmol photons m^{-2} s^{-1})
350
300
250
200
150
100
50
0
Time (h)
(e)
PSII/PSI
1.40
1.20
1.00
0.80
0.60
0.40
0.20
0.00
LL
ML
(f)
Photosynthetic electron
flow (e^- s^{-1})
LL
ML

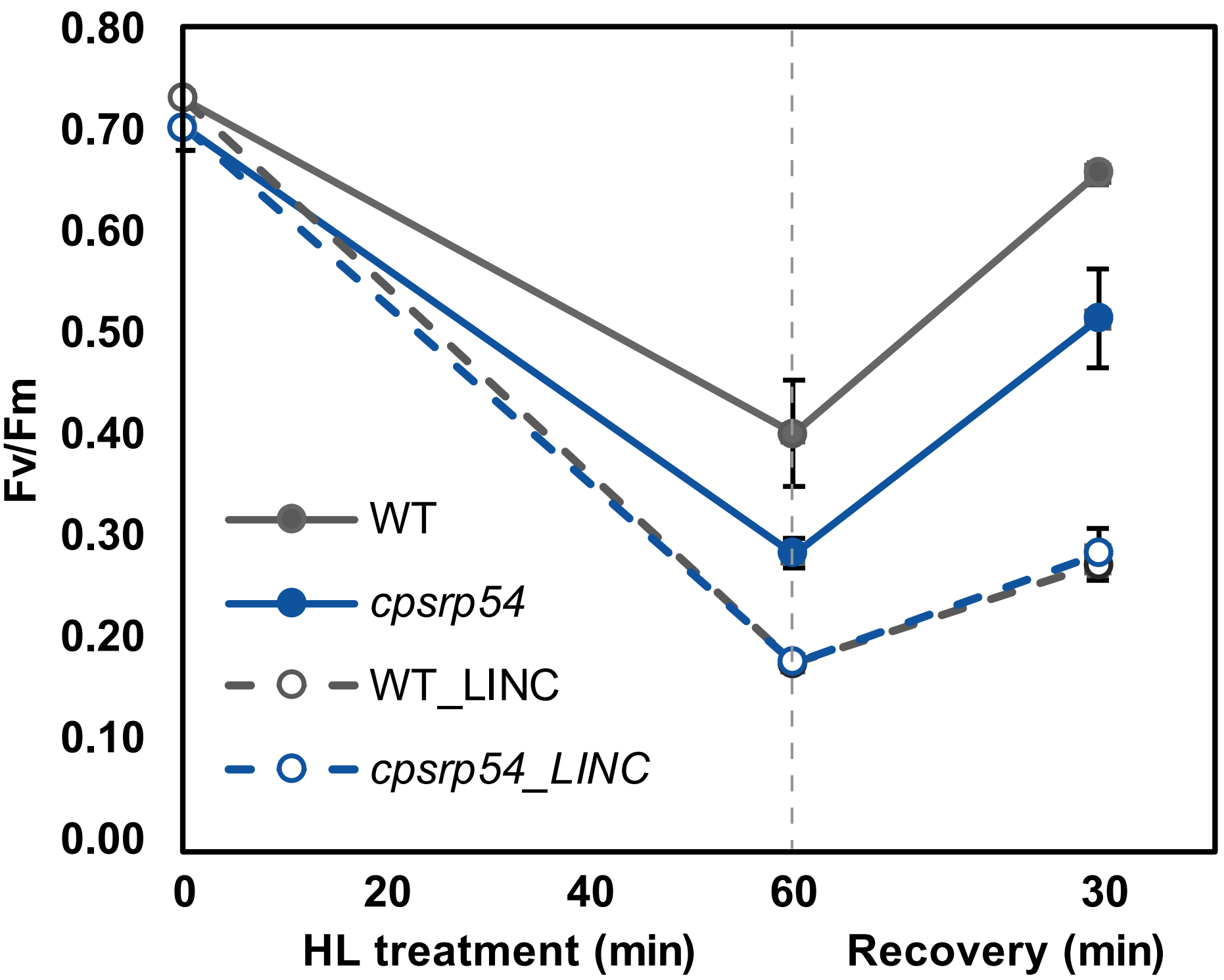
0.80
0.70
0.60
0.50
0.40
0.30
0.20
0.10
0.00
Fv/Fm
WT
cpsrp54
WT_LINC
cpsrp54_LINC
0
20
40
60
30
HL treatment (min)
Recovery (min)

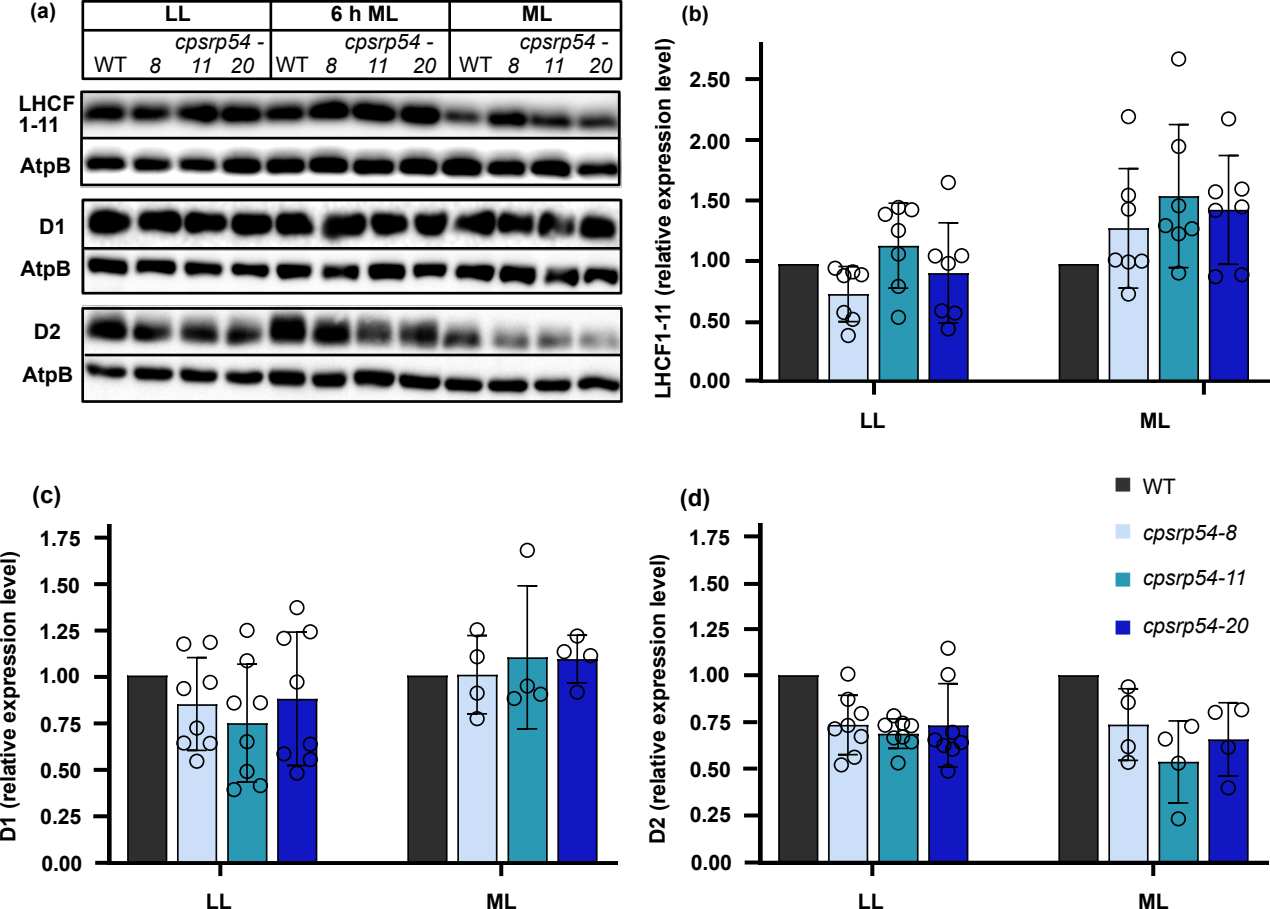
(a)
LL
6 h ML
ML
WT
cpsrp54 - 8
cpsrp54 - 11
cpsrp54 - 20
LHCF 1-11
AtpB
D1
AtpB
D2
AtpB
(b)
LHCF1-11 (relative expression level)
2.50
2.00
1.50
1.00
0.50
0.00
LL
ML
(c)
D1 (relative expression level)
1.75
1.50
1.25
1.00
0.75
0.50
0.25
0.00
LL
ML
(d)
D2 (relative expression level)
1.75
1.50
1.25
1.00
0.75
0.50
0.25
0.00
LL
ML
WT
cpsrp54-8
cpsrp54-11
cpsrp54-20

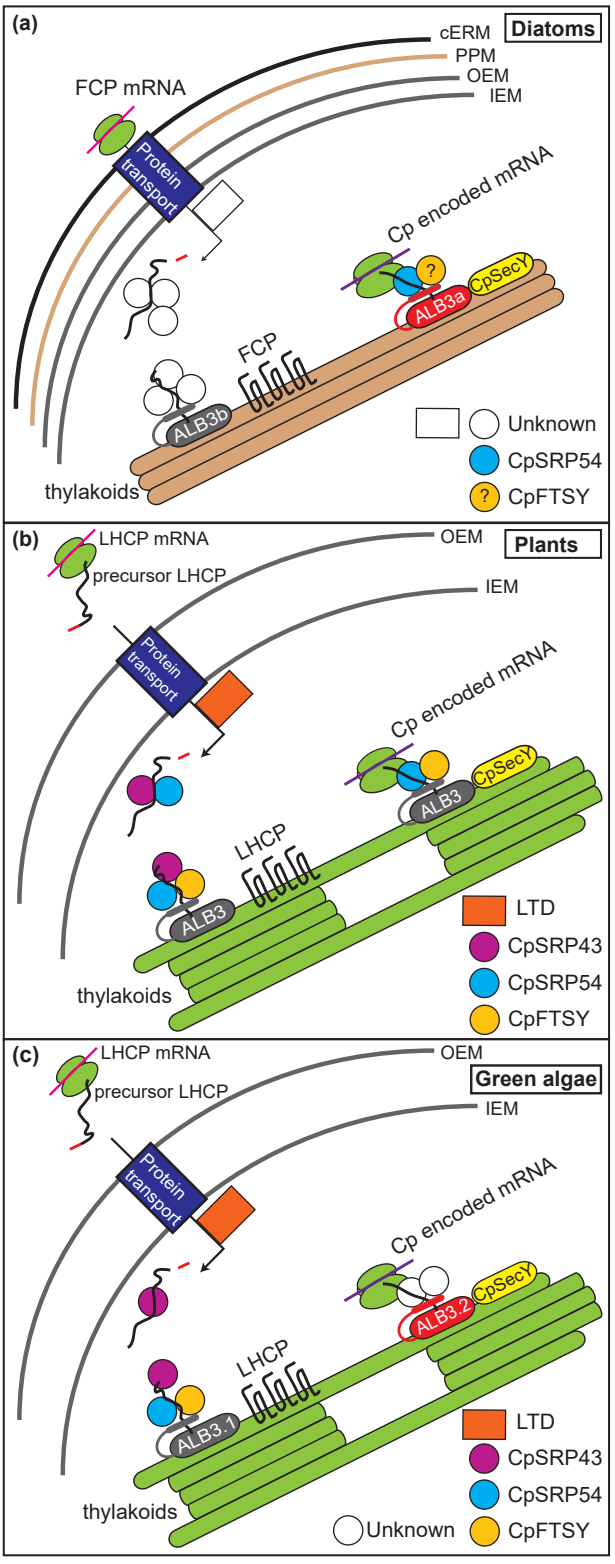
(a)
Diatoms
cERM
PPM
OEM
IEM
FCP mRNA
Protein transport
Cp encoded mRNA
?
CpSecY
ALB3a
FCP
ALB3b
Unknown
CpSRP54
?
CpFTSY
thylakoids
(b)
Plants
LHCP mRNA
precursor LHCP
OEM
IEM
Protein transport
Cp encoded mRNA
CpSecY
ALB3
LHCP
ALB3
LTD
CpSRP43
CpSRP54
CpFTSY
thylakoids
(c)
Green algae
LHCP mRNA
precursor LHCP
OEM
IEM
Protein transport
Cp encoded mRNA
CpSecY
ALB3.2
LHCP
ALB3.1
LTD
CpSRP43
CpSRP54
CpFTSY
thylakoids
Unknown